

2

NASA TMX 63692

VHF SATELLITE NAVIGATION SYSTEM

N69-38637

FACILITY FORM 602

(ACCESSION NUMBER)	(THRU)
92	1
(PAGES)	(CODE)
Inv-63692	2
(NASA CR OR TMX OR AD NUMBER)	(CATEGORY)



JANUARY 1968



GODDARD SPACE FLIGHT CENTER
GREENBELT, MARYLAND

Reproduced by the
CLEARINGHOUSE
 for Federal Scientific & Technical
 Information Springfield Va 22151

VHF SATELLITE NAVIGATION SYSTEM

January 1968

GODDARD SPACE FLIGHT CENTER
Greenbelt, Maryland

TABLE OF CONTENTS

Section	Title	Page
1.0	Introduction	1
2.0	Experiment Description	5
3.0	System Description	9
3.1	Ground Control Center	10
3.2	Reference Terminal	14
3.3	Aircraft Terminal	16
4.0	VHF Sidetone Ranging	17
4.1	VHF Range Resolution	17
4.2	Range Ambiguity	21
4.3	VHF Link Considerations	22
4.4	Ionospheric Compensation	31
4.5	Velocity Considerations	40
5.0	Position Location	41
6.0	Error Analysis	47
6.1	VHF Range Measurement Errors	47
6.2	Altitude Measurement Error	53
6.3	Satellite Position Error	53
6.4	Position Location Accuracy	55
7.0	Management	59
8.0	Schedule	61
9.0	References	63
Appendix		
A.	A Comparison Between Ranging Tones and PN (Pseudo-Noise) Codes for Commercial Air Traffic Control	
B.	Atmospheric Bias Errors in VHF Ranging	
C.	Distance from the Aircraft to the Center of the Earth	
D.	Altitude Measurement Errors	

LIST OF ILLUSTRATIONS

Figure	Title	Page
2-1	VHF Satellite Navigation System Configuration	6
3-1	Sidetone Ranging Pattern	11
3-2	Functional Block Diagram of GCC	12
3-3	Block Diagram of Reference Terminal Transponder . .	15
3-4	Aircraft Terminal Configuration	16
4-1	Functional Block Diagram of VHF Range Measurement	18
4-2	RMS Range Error Due to Phase Error as a Function of SNR	20
4-3	Ambiguity Resolution Versus Phase Noise	23
4-4	Noise Power Density/Link Loss (N_a/L_{as})—Satellite to Aircraft	25
4-5	Noise Power Density/Link Loss (N_g/L_{ag})—Satellite to Ground	27
4-6	Noise Power Density/Link Loss (N_s/L_{as})—Aircraft to Satellite	29
4-7	Noise Power Density/Link Loss (N_s/L_{gs})—GCC to Satellite	30
4-8	Tropospheric Bias Versus Elevation Angle	33
4-9	Magnitude of Ionospheric Bias Term as a Function of Integrated Electron Density	34
4-10	The Variation with Magnetic Dip of the Monthly Media Local Noon Values of $N_m F_2$ for Different Months	37
4-11	The Variation with Magnetic Dip of the Monthly Median Values of $N_m F_2$ at Different Hours of the Day in December 1957	37
4-12	Comparison of Columnar Electron Content Versus Time Curves Obtained from Syncom III at Hawaii and Stanford	38
4-13	Comparison of Columnar Electron Content Versus Time Curves Obtained from ATS-1 at Ely and Stanford	39
5-1	Geometrical Relation Between the Earth, Satellites, and Aircraft Terminal	42
6-1	Bottom-to-Top Rejection Ratio of DMC33-2 Antenna (Horizontal Polarization)	50
6-2	Bottom-to-Top Rejection Ratio of DMC33-2 Antenna (Vertical Polarization)	51
6-3	Multipath RMS Phase Error Without Smoothing	54
8-1	Experiment Schedule	61

VHF SATELLITE NAVIGATION SYSTEM

1.0 INTRODUCTION

The ever-increasing need for an improved air traffic control system, particularly over the North Atlantic area, has spurred an intense search for system concepts and techniques which will satisfy the future requirements of commercial air traffic. This proposal describes a VHF Satellite Navigation Experiment which can be conducted using previously developed technology, equipments, and the ATS-1 and ATS-3 satellites presently in orbit. The primary goal of this experiment is to determine the position location accuracy that can be achieved and to define confidence levels that can be attained by ranging to geosynchronous satellites at VHF frequencies. A secondary goal is to demonstrate that aircraft positions can be determined by these means in real time under flight conditions.

Another potential application of this VHF Satellite Navigation System is location and tracking of balloon-borne meteorological platforms. Recommendations and studies concerning the feasibility of a Global Weather Observing System indicate that an experiment to demonstrate such a position location capability would be meaningful and potentially important. This demonstration would be particularly significant because the position location is accomplished via geosynchronous satellites.

A limiting parameter which must be considered in the design of an air traffic control system, as well as a global meteorological balloon system, is the satellite bandwidth requirements per aircraft or balloon to be serviced. As discussed in subsequent sections of this document, the proposed sidetone ranging technique requires a significantly lower satellite bandwidth than that required by other ranging schemes of comparable accuracy and resolution. Additionally, the specific sidetone pattern proposed for this experiment represents a near-optimum configuration for sidetone ranging to geosynchronous satellites when considering ranging accuracy requirements, range ambiguity resolution, satellite bandwidth requirements, allowable acquisition time, etc. Although sidetone ranging has been selected as the means for range measurements, the experiment has been designed to investigate fundamental limitations and statistical characteristics which are independent of the range measurement technique.

The VHF Satellite Navigation System described herein utilizes the technology and equipment developed for the Omega Position Location Equipment (OPLE) Experiment, and it employs

the Applications Technology Satellites (ATS-1 and ATS-3) for relay between the Ground Control Center (GCC) and cooperating aircraft. The GCC has the capability of determining the unambiguous location of each cooperating aircraft, provided the aircraft is within the area of simultaneous coverage by the ATS-1 and ATS-3 satellites, and determination of the aircraft position is not dependent upon another system (such as LORAN or OMEGA)

The data processing functions performed by the OPLE Control Center in the present OPLE Experiment are almost identical to the sidetone processing functions that are required of the GCC for the proposed experiment. In addition, the self-check tones presently generated by the OPLE Control Center represent a near-optimum tone configuration for sidetone ranging to synchronous satellites. As a result, the OPLE Control Center hardware and software can be used to perform this VHF Satellite Navigation Experiment with only a few modifications to the existing equipment being required. These modifications can be made without affecting the functions that are required of the OPLE Control Center by the OPLE Experiment.

This VHF sidetone ranging experiment is a logical extension of the OPLE Experiment. Also, the sidetone ranging technique described herein is very similar to the ranging technique used in the proposed Position Location and Aircraft Communication Equipment (PLACE) Experiment described in Goddard Space Flight Center Document No X-731-67-159, thus, the results obtained in this VHF sidetone ranging experiment can be incorporated into the design of the PLACE system. Just as with the existing OPLE system hardware, this experimental VHF Satellite Navigation System is not designed to be directly expandable into an operational system, however, the information provided by this experiment will most certainly be useful in the subsequent design of any operational air traffic control system.

Position location in the proposed system is accomplished by means of simultaneous ranging from two geosynchronous satellites to an aircraft of known altitude. This ranging scheme utilizes the unmodified VHF sidetone pattern that is presently generated in the OPLE Control Center for self-check purposes. From the measured ranges between the aircraft and the ATS-1 and ATS-3 satellites, two spheres are defined. These spheres are centered at the two satellite positions and they include the aircraft position. Similarly, a sphere is defined from the known aircraft altitude relative to the center of the Earth. This third sphere is concentric with the Earth and also includes the aircraft position. The intersections of these three spheres define two possible aircraft positions which are symmetrical about the Earth's equator. The position ambiguity between the Northern and Southern hemispheres can be readily

resolved from a priori knowledge for all flight paths other than those near or crossing the Earth's equator. For these cases, position ambiguity can be resolved by continuous tracking of the aircraft position from a known starting point

Range measurements from the aircraft to the two ATS satellites are performed simultaneously in this experiment; however, only one sidetone pattern (one data channel) is transmitted to the ATS-1 satellite during a range measurement. This is mandatory to avoid the intermodulation distortion which results from the hard limiter in the ATS-1 satellite transponder when a multiplicity of signals exists. As a result, the aircraft terminal can be channelized to receive on a given channel frequency and to transmit at another channel frequency. In an operational system, this would minimize the bandwidth requirements for each aircraft, thereby maximizing the number of aircraft that could be serviced simultaneously with a particular satellite bandwidth. Additionally, only one transponder is required in the aircraft terminal to perform simultaneous range measurements to two satellites, thus, the terminal hardware requirements are kept to an absolute minimum. This hardware reduction would be of utmost importance for data collection platforms to be used with meteorological balloons.

This experimental VHF ranging system consists of (1) a modified OPLE Control Center, including a second VHF antenna, which functions as the Ground Control Center, (2) an aircraft terminal, and (3) a reference terminal and satellite transponder simulator which will be used for system calibration purposes. The system will also utilize the VHF transponders in the ATS-1 and ATS-3 satellites. The GCC will be capable of receiving and processing either VHF ranging data or OPLE data, therefore, the present OPLE Experiment and the proposed VHF Satellite Navigation Experiment can be conducted concurrently if desired; however, a brief down time is required to switch from one experiment to the other

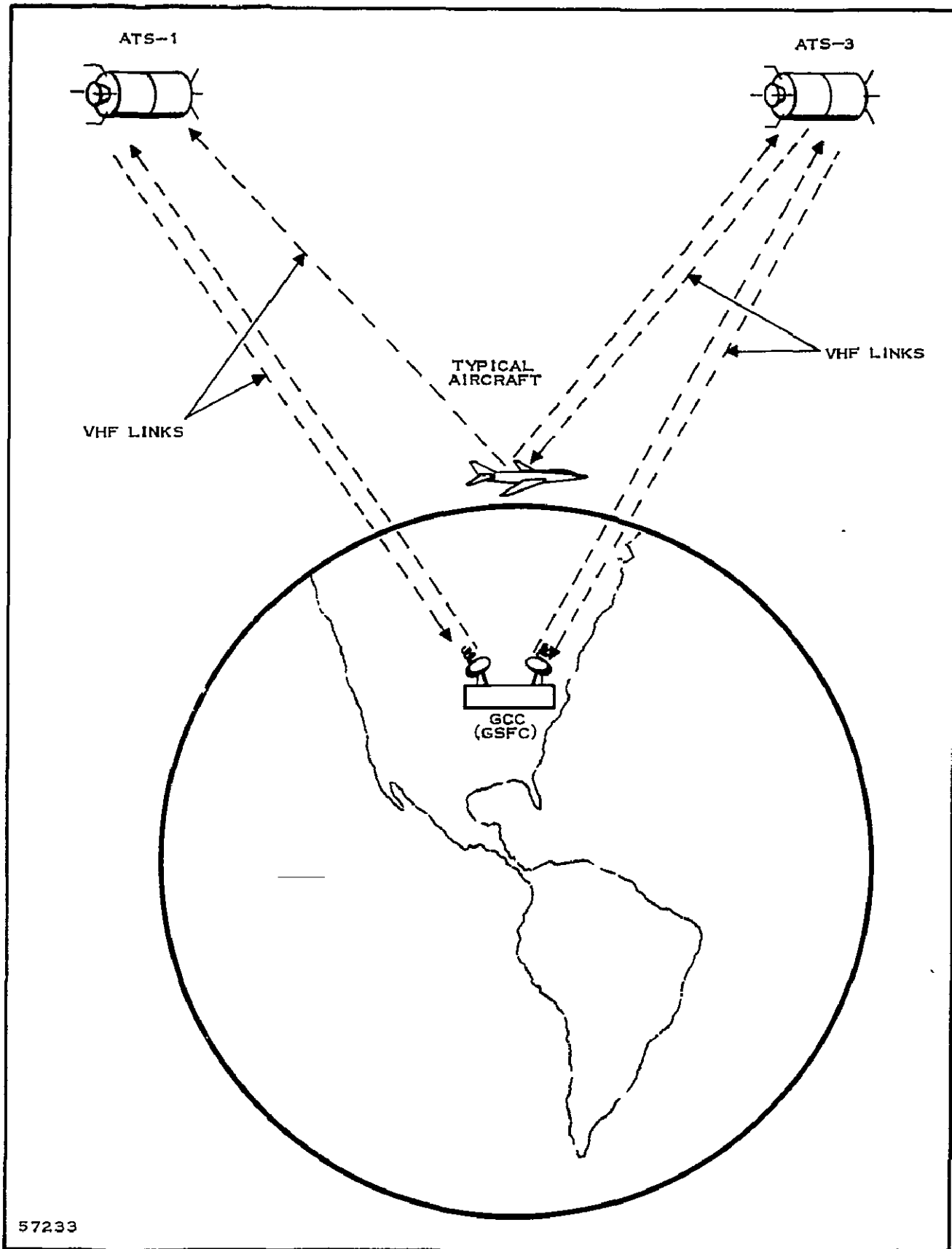
2.0 EXPERIMENT DESCRIPTION

The primary objective of this VHF Satellite Navigation Experiment is to determine the accuracy and reliability limitations of locating the positions of aircraft (or remote platforms) by means of VHF sidetone ranging measurements to synchronous satellites. The range measurements are made from a Ground Control Center (GCC) located at Goddard Space Flight Center to cooperating aircraft via VHF links through the ATS-1 and ATS-3 satellites. The resulting range data is combined with known aircraft altitude information to locate the position of the aircraft. The experiment can be performed with an FAA aircraft, commercial air freight aircraft, or any other suitable aircraft that is available. Aircraft performance characteristics, such as speed, are not limiting factors.

The experiment configuration is shown in Figure 2-1. The GCC transmits VHF ranging tones to the ATS-3 satellite which relays the tones back to the Ground Control Center and to cooperating aircraft. The aircraft terminal receives the ranging tones from the ATS-3 satellite and retransmits them simultaneously to the GCC via the ATS-1 and ATS-3 satellites. The GCC receives and demodulates the ranging tones from the ATS-1 and ATS-3 satellites and compares the delay of each to the delay of the ranging tones that were transmitted by the GCC. The delay differences between the received and transmitted tones represent the various VHF path lengths between the GCC, the ATS satellites, and the aircraft. These simultaneous range measurements, along with a similar but separate range measurement from the GCC to the ATS-1 satellite, are used to determine the ranges from the aircraft to the ATS-1 and ATS-3 satellites.

As indicated above, this experiment employs the VHF transponders in the ATS-1 and ATS-3 satellites. Each transponder has transmit and receive frequencies of 135.6 MHz and 149.22 MHz, respectively. Similarly, a VHF transponder is required in the aircraft terminal, although it is inverted to provide transmit and receive frequencies of 149.22 MHz and 135.6 MHz, respectively. The GCC consists of the present OPLE Control Center, slightly modified for this experiment, however, the functions required of the OPLE Control Center by the OPLE Experiment are retained. This permits concurrent performance of the VHF Satellite Navigation Experiment and the OPLE Experiment, if desired.

The ranging method proposed for this VHF Satellite Navigation Experiment is the sidetone ranging technique. Three non-harmonic tones of appropriate frequency are transmitted with a



57233

Figure 2-1. VHF Satellite Navigation System Configuration

reference carrier and then used in such a manner that the desired ranges can be determined unambiguously. The ranges measured between the aircraft and the ATS-1 and ATS-3 satellites define two spheres centered at the satellite positions, and a third sphere is defined by the known aircraft altitude above the center of the Earth. The position of the aircraft is determined by means of digital computer processing of the measured VHF range data and the known aircraft altitude information.

Another possible application of the VHF Satellite Navigation System involves meteorological balloons that are currently being launched from Palestine, Texas, by the National Center for Atmospheric Research (NCAR). A balloon-borne terminal could be launched in the January-March 1969 time period when prevailing westerly winds would place the balloon in simultaneous view of the ATS-1 and ATS-3 satellites, and the balloon could then be tracked by the GCC to measure the wind velocity at the balloon's flight altitude (approximately 20 kilometers).

The absolute position location accuracy of this VHF sidetone ranging system is determined primarily by the uncertainty of the ionosphere. Improved ionospheric prediction techniques are currently being developed, however, by using presently available ionospheric data to compute bias errors, it is estimated that a worst-case absolute position location accuracy on the order of ± 2.0 kilometers (± 1.08 nautical miles) can be achieved. For a differential (relative) position location measurement, such as that required in an air traffic control system, the ionospheric bias errors are common. In this case, the estimated worst-case error is on the order of ± 0.7 kilometer (± 0.38 nautical mile), provided the distance between the two aircraft is within approximately 100 kilometers.

3.0 SYSTEM DESCRIPTION

Position location of an aircraft (or remote platform) in the VHF Satellite Navigation System is accomplished by first determining the distance from the aircraft to the center of the Earth and the ranges from the aircraft to the ATS-1 and ATS-3 satellites. This altitude and range data is then processed off-line to (1) resolve the range ambiguities, (2) correct for system bias errors, and (3) determine the aircraft position. Controlled portions of this experiment will be performed with the aircraft altitude known to good precision. Hence, the distance from the aircraft to the Earth's center can be determined by an iterative process as described later, and other factors contributing to position uncertainties can be investigated separately. Therefore, the primary function of the VHF Satellite Navigation System in this experiment is to measure the aircraft-to-satellite ranges and to compute the aircraft position.

The distances from the aircraft to the ATS satellites are measured indirectly by means of a VHF sidetone ranging technique. In this system, a set of three non-harmonic VHF ranging tones and a reference carrier are generated at the GCC and transmitted to the ATS-3 satellite at 149.22 MHz. The ATS-3 satellite translates this ranging tone pattern to 135.6 MHz, maintaining the original tone phase relationship, and relays the ranging tones back to the GCC and also to an aircraft. The return ranging tones are received and processed by the GCC to determine the unambiguous two-way range from the GCC to the ATS-3 satellite; this range is represented by the differences in phases of the received and transmitted ranging tones at the GCC. The aircraft also receives the 135.6-MHz ranging tone pattern from the ATS-3 satellite and translates it to 149.22 MHz without altering the tone phase relationships. The ranging tones are then relayed back to the GCC via the ATS-1 and ATS-3 satellites. The GCC receives and processes the two tone patterns from the satellites to determine (1) the unambiguous two-way range from the GCC to the aircraft via the ATS-3 satellite, and (2) the unambiguous one-way range from the GCC to the aircraft via the ATS-3 satellite and the return from the aircraft to the GCC via the ATS-1 satellite. In a similar but separate measurement, the GCC transmits the sidetone pattern to the ATS-1 satellite. The return signal from the satellite is then received and processed by the GCC to determine the unambiguous two-way range from the GCC to the ATS-1 satellite. Finally, the distances from the aircraft to the ATS-1 and ATS-3 satellites are computed using range differences derived from the above series of range measurements.

The computed distances from the aircraft to the ATS satellites are processed off-line to remove the ranging errors due to

ionospheric effects and other system bias components. These corrected ranges are then combined with known aircraft altitude data to obtain the aircraft position.

This VHF Satellite Navigation Experiment employs a Ground Control Center, a reference terminal, an aircraft terminal, the ATS-1 and ATS-3 satellites, a satellite transponder simulator, an off-line digital computer, and at least one cooperating aircraft. The present OPLE Control Center can be modified and used as the GCC, whereas the aircraft and reference terminals can be constructed from modified commercial equipment. The remaining equipment will be available for use in the experiment.

3.1 Ground Control Center (GCC)

The GCC must generate the required VHF ranging tones, transmit these tones to the ATS-3 satellite or ATS-1 satellite as required, and then receive and process the return signals to determine the phase differences between the transmitted and received ranging tones. In addition, the GCC must perform all the functions that are presently required by the OPLE Experiment. It will be shown that the additional capability can be provided by relatively minor modifications of the existing OPLE Control Center (OCC).

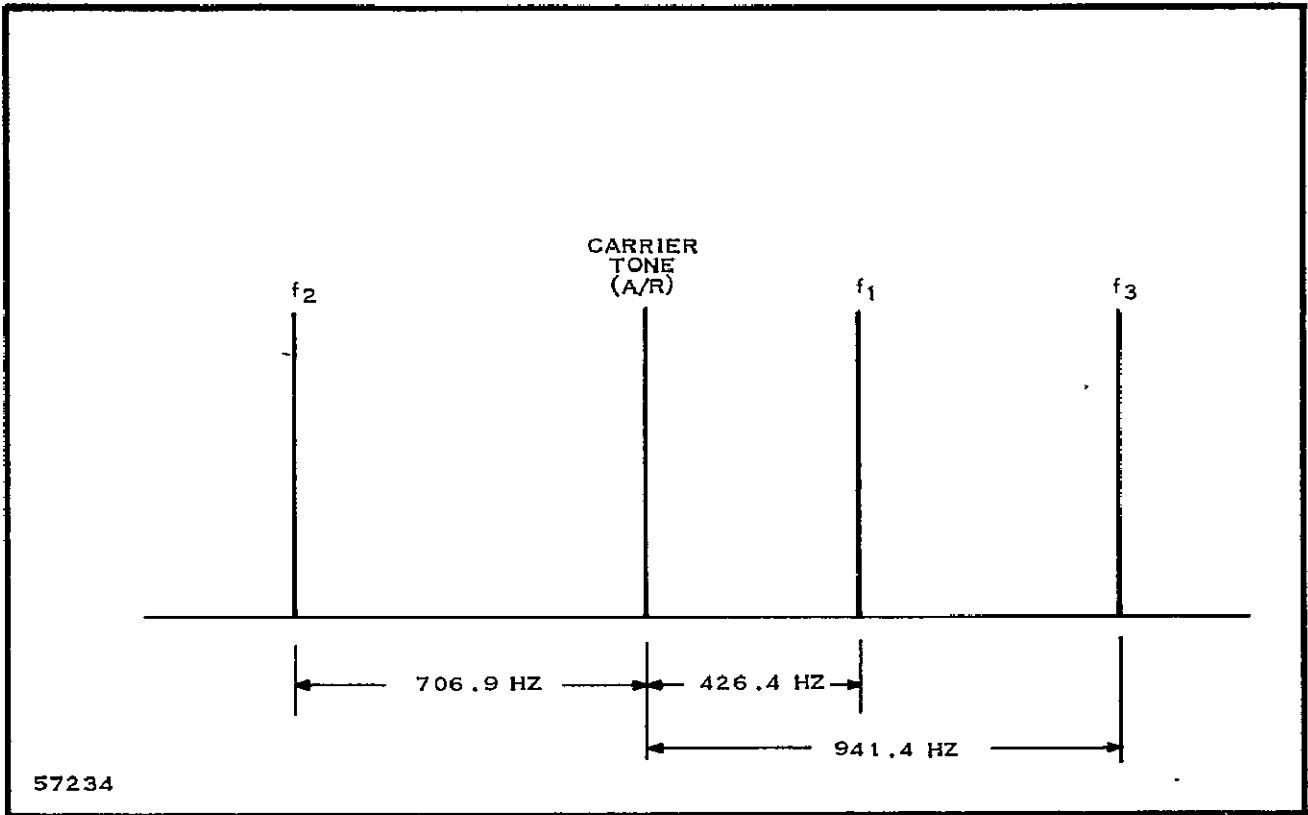
3.1.1 Ranging Tone Generation

The self-check subsystem in the GCC generates a channel of simulated OPLE Platform Electronics Package (PEP) data. This simulated PEP data includes an acquisition/reference tone (carrier) and three frequency-translated Omega tones (Figure 3-1) which function as the ranging tones in this VHF ranging experiment. In the OPLE Experiment, these tones are commutated in synchronization with the Omega Navigation System timing and then transmitted to the ATS-3 satellite; the return signal from the satellite is received and processed by the GCC to determine the phase differences between the received and transmitted tones. This is identical to the tone processing that is required in this proposed VHF Satellite Navigation System.

To enable VHF sidetone ranging measurements via the two satellites, the GCC self-check subsystem must be modified to provide an alternate mode of operation in which the three simulated Omega tones are continuous rather than commutated. This modification consists of relatively minor wiring changes.

3.1.2 RF Electronics Subsystem Modification

As described in Section 3.0, continuous range measurements to an aircraft are performed by transmitting ranging tones to the



57234

Figure 3-1. Sidetone Ranging Pattern

ATS-3 satellite while simultaneously receiving return ranging tones from the ATS-1 and ATS-3 satellites. Hence, dual VHF antennas and receivers must be incorporated into the GCC as shown in Figure 3-2. The return ranging tones that are received by direct translation from the ATS-3 satellite are assigned a channel frequency different from that used to relay the ranging tones to the aircraft. However, the two sets of ranging tones received at the GCC from the aircraft via the ATS-1 and ATS-3 satellites occupy the same channel, with the necessary isolation between these two signals being provided by the GCC antennas. Additional isolation is provided because of the difference in the two satellite transponder "side-step" frequencies. Because of this relatively large difference in the "side-step" frequencies of the two satellites, separate VHF frequency synthesizers must also be included for the two VHF receivers in the GCC.

The GCC receivers extract the relative phase data from the return ranging tones. The first step of this extraction process is to remove the random phase shifts which result from the series string of frequency translation elements in the VHF paths. These random phase shifts apply equally to all ranging tones, including the carrier, thus their effect can be removed by phase-locking to the reference tone. This is accomplished in the OPLE receivers that follow the

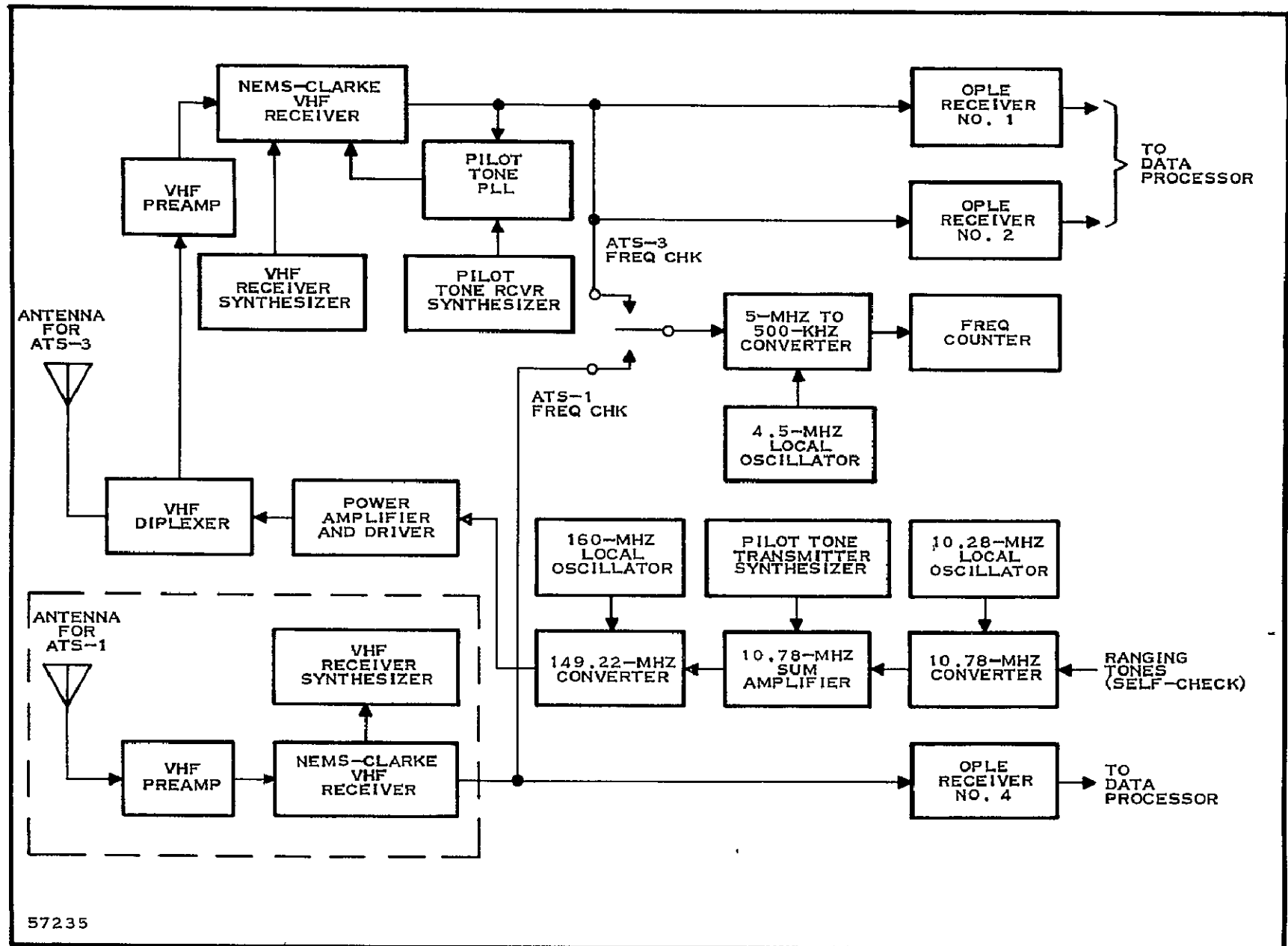


Figure 3-2. Functional Block Diagram of GCC

VHF receivers. After the phase jitter has been removed, the phases of the three received ranging tones are compared to the phases of the ranging tones transmitted by the GCC, and the resulting phase angles constitute the basic ranging data.

For the separate range measurement to the ATS-1 satellite, the ATS-3 antenna at the GCC is positioned to point at the ATS-1 satellite and the ranging tones are transmitted to it. The return tones from the ATS-1 satellite are received at the GCC by the ATS-1 antenna and receiver because the desired satellite "side-step" frequency error compensation has already been introduced into this receiver.

A functional GCC block diagram illustrating the required OPLE Control Center modifications is shown in Figure 3-2, with the added equipment enclosed in the dashed lines. It is significant to note that the ATS-3 receiver at the GCC requires a pilot tone tracking phase-lock loop to remove the excessive frequency jitter that is inserted by the ATS-3 satellite. This is not necessary in the ATS-1 receiver at the GCC, as was demonstrated during the successful OPLE Engineering Tests with the ATS-1 satellite.

3.1.3 Timing and Control Modifications

Because the system timing and data processing requirements are slightly different for the VHF ranging mode of operation, minor modifications to the control electronics subsystem in the GCC will be required. These modifications consist only of wiring changes. The OPLE system software will not have to be changed for this experiment, however, a modification to it would allow a reduction in the ranging tone processing time.

3.1.4 Off-Line Data Processing

The off-line data reduction and data processing required to locate an aircraft by means of VHF sidetone ranging is entirely different from that required for position location by means of the OPLE technique. Consequently, additional off-line software must be developed for the VHF Satellite Navigation Experiment.

3.1.5 OPLE Experiment Compatibility

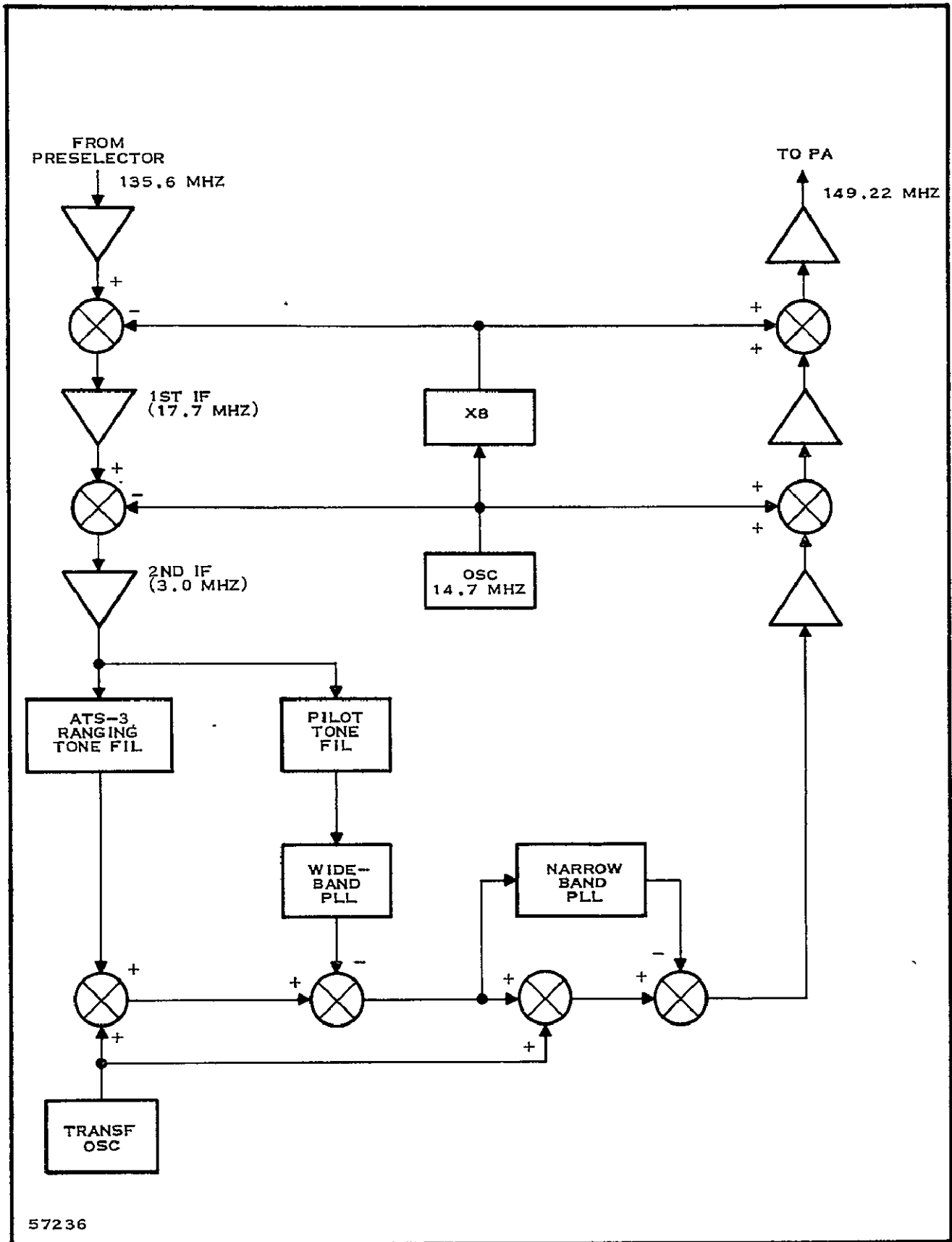
The GCC described herein is an OPLE Control Center with the necessary modifications included to provide the additional capability required to perform the VHF ranging experiment along with the OPLE Experiment. Equipment, wiring, and software changes are minor, and they can be made in such a way that only a few minutes

down time will be required to switch from one experiment to the other. The GCC can be used to perform both experiments, thus providing the capability of making nearly simultaneous position location measurements for comparison of the two position determining techniques.

3.2 Reference Terminal

The reference terminal is comprised of a VHF transponder and a VHF antenna, it can be used by the GCC operator to verify proper operation of the VHF Satellite Navigation System and to perform system calibration without relying on the aircraft terminal. The reference terminal can be located near the GCC or it can be installed at a remote ground facility; however, in either case, adequate coverage by both ATS satellites must be provided. This terminal can be used at the remote location to perform differential position location measurements in conjunction with the aircraft terminal, and it can also be used for ionospheric error studies.

A block diagram of the reference terminal transponder is shown in Figure 3-3. It consists of a double-conversion VHF receiver which receives and amplifies the VHF ranging tones and pilot tone that are relayed from the GCC via the ATS-3 satellite. The ranging tones and pilot tone are separated by band-pass filters. Then, a two-step phase jitter suppression operation follows to completely remove the phase jitter that is introduced in the ranging tones by the ATS-3 satellite and the VHF links. The necessity for doing this has already been demonstrated in the OPLE Experiment, and the required OPLE Control Center modifications have been made to accommodate the frequency jitter acquired in a one-way pass through the ATS-3 satellite. In the first jitter suppression stage, phase-lock to the pilot tone is acquired by a wideband phase-lock loop, thus the group phase jitter is tracked out. This includes any doppler shift frequency, satellite "side-step" frequency error, satellite frequency jitter, or other phase jitter. The ranging tones are next applied to a narrowband phase-lock loop which acquires lock to the reference tone and thus tracks out any phase jitter on the reference tone relative to the pilot tone. The jitter-free ranging tones are then up-converted and transmitted at a power level of 100 watts. To prevent saturation of the transponder receiver by the power amplifier, approximately 70 dB of isolation is provided by the pre-selector between the antenna and the receiver. Because the VHF transponder may be required to operate in the vicinity of high-power transmitters, a high level of image rejection is necessary, hence the double-conversion receiver technique is employed.



57236

Figure 3-3. Block Diagram of Reference Terminal Transponder

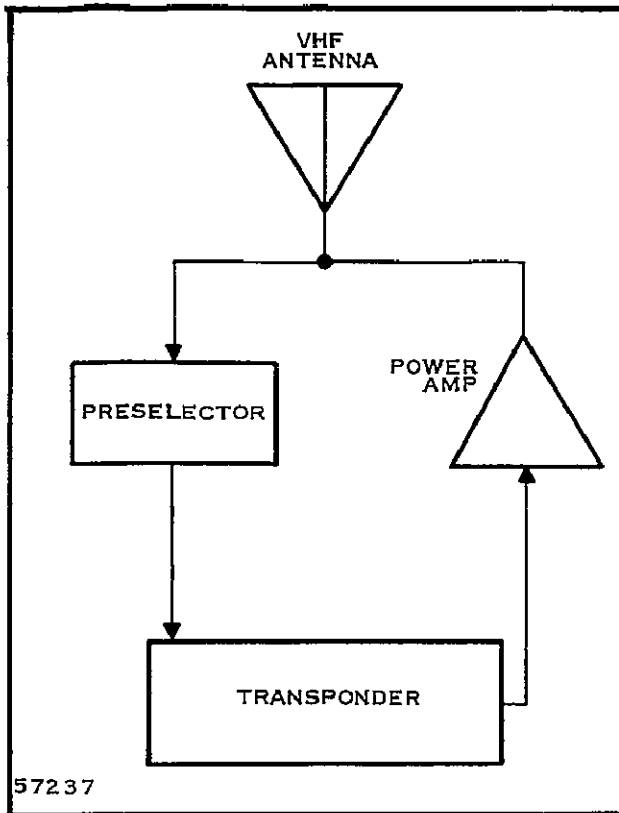


Figure 3-4. Aircraft Terminal Configuration

The reference terminal will be constructed from commercial equipment with the exception of the phase-lock loops, which will be of the type presently used in the OPLE Control Center.

3.3 Aircraft Terminal

The aircraft terminal for the VHF Satellite Navigation System consists of a VHF transponder (which is a ruggedized version of that used in the reference terminal) and a VHF aircraft antenna (Type DMC 33-2). This equipment, shown in block diagram form in Figure 3-4, can be installed in a cooperating aircraft. The operation of the transponder is as outlined in Section 3.2.

The aircraft can also be equipped to operate in the OPLE mode if desired. In this OPLE mode of operation (VHF sidetone ranging not performed), a PEP is

utilized as the aircraft terminal. This mode of operation is identical to the OPLE system operation in that the PEP (1) responds to coded interrogations from the GCC via the ATS-3 satellite, (2) encodes and transmits sensor data to the GCC via a return link through the satellite, (3) receives and conditions the VLF tones transmitted by the Omega Navigation System, and (4) up-converts the Omega tones to the VHF link frequency and transmits them to the GCC via the ATS-3 satellite.

4.0 VHF SIDETONE RANGING

Location of the position of an aircraft in this navigation system depends on four VHF range measurements. The range measurements are shown in Figure 2-1 and include:

- (1) The path length from the GCC to the ATS-3 satellite and back ($2R_{g3}$)
- (2) The path length from the GCC to the aircraft and back via the ATS-3 satellite ($2R_{g3a}$)
- (3) The path length from the GCC to the aircraft via the ATS-3 satellite and back to the GCC via the ATS-1 satellite and back (R_{g3a1g})
- (4) The path length from the GCC to the ATS-1 satellite and back ($2R_{g1}$).

The first three range measurements are made simultaneously and the fourth is made on a time-shared basis. The primary justification for time-sharing the range measurements is that potential multiple access difficulties due to the ATS-1 satellite hard-limiting transponder can be avoided. Furthermore, the ATS-1 satellite is nominally stationary and its dynamic behaviour is such that frequent measurements of the range from the GCC to the ATS-1 satellite are completely adequate. This approach also allows the use of minimal hardware in the aircraft transponder and at the GCC.

Since the range measurements are made at VHF, the range estimates are perturbed by ionospheric effects. However, it is possible to correct for some of these errors, thus making a VHF Satellite Navigation Experiment possible with relatively high accuracy being achieved. A functional block diagram showing the operations leading to a VHF range measurement is shown in Figure 4-1.

The ranging method used in this system is the sidetone ranging technique. This is one of the two techniques usually considered for ranging between a fixed station and a cooperative target; the other standard ranging technique employs a pseudo-noise (PN) code. In Appendix A, the relative merits of these two ranging techniques are discussed using the criteria proposed by Baghdady and Kruse (Reference 1). It is shown conclusively that sidetone ranging is the preferred technique for this application.

4.1 VHF Range Resolution

The range value for each of the four measurement paths in this VHF Satellite Navigational System is determined from simultaneous phase measurements of the three sidetones (426 Hz, 707 Hz, and 941 Hz).

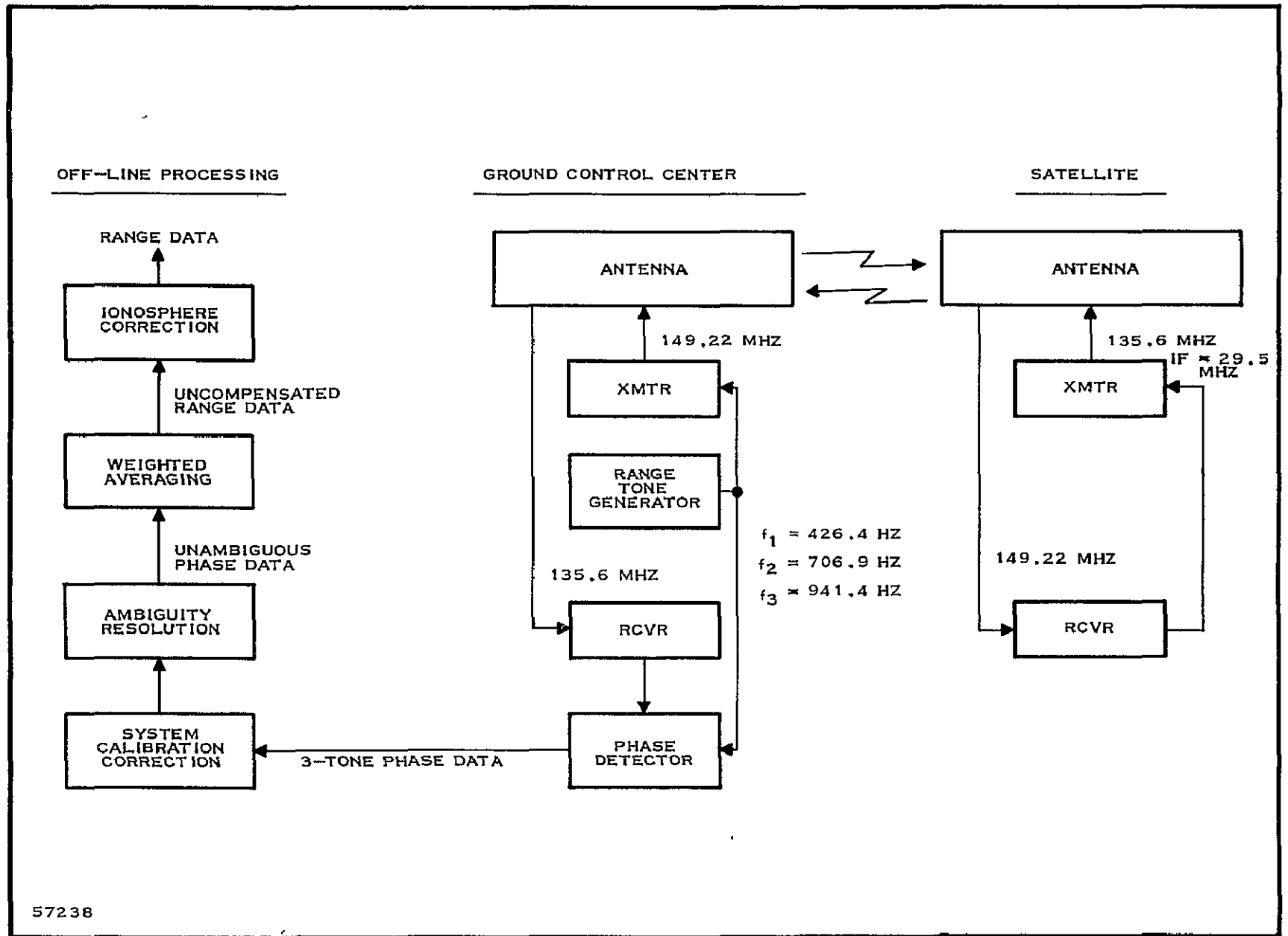


Figure 4-1. Functional Block Diagram of VHF Range Measurement

These phase measurements represent the phase shifts of the respective sidetones due to their transmission through the path of unknown range. The range (R) is related to the phase shift (θ) and the sidetone frequency (f) by the equation:

$$R = \frac{c\theta}{f}, \text{ where } c \text{ is the propagation velocity.}$$

The range resolution is limited by the phase measurement accuracy and is inversely proportional to the sidetone frequency. A plot of the RMS range error due to noise for each of the sidetone frequencies is shown in Figure 4-2. Included in this figure is a plot of the range error which results from the best weighted-average of the three independent range measurements. A typical value of phase signal-to-noise ratio for this system is 37 dB, yielding RMS range errors of 520, 320, 230, and 180 meters for the 426-Hz tone, 707-Hz tone, 941-Hz tone, and the best weighted-average, respectively. Factors which contribute to the phase noise include atmospheric noise, multipath effects, and system calibration inaccuracies. A detailed discussion of these various factors, with their resulting range errors, is presented in Section 6.1.

The best weighted-average of the three measurements is computed to minimize the range error. This minimum error is attained by applying weighting functions proportional to the measurement accuracies, which in the case of constant phase jitter due to noise, becomes proportional to the sidetone frequencies. In other words, the general weighted-average range is expressed by the equation:

$$\bar{R} = \frac{c \left[\frac{\theta_1}{f_1} K_1 + \frac{\theta_2}{f_2} K_2 + \frac{\theta_3}{f_3} K_3 \right]}{K_1 + K_2 + K_3}$$

where the optimum values of K are:

$$\begin{aligned} K_1 &= f_1 \\ K_2 &= f_2 \\ K_3 &= f_3. \end{aligned}$$

With these weighting values, the equation becomes:

$$\bar{R} = \frac{c \left[\theta_1 + \theta_2 + \theta_3 \right]}{f_1 + f_2 + f_3} .$$

This best weighted-average gives an equivalent 2 dB improvement over the accuracy that could be attained from the 941-Hz measurement alone.

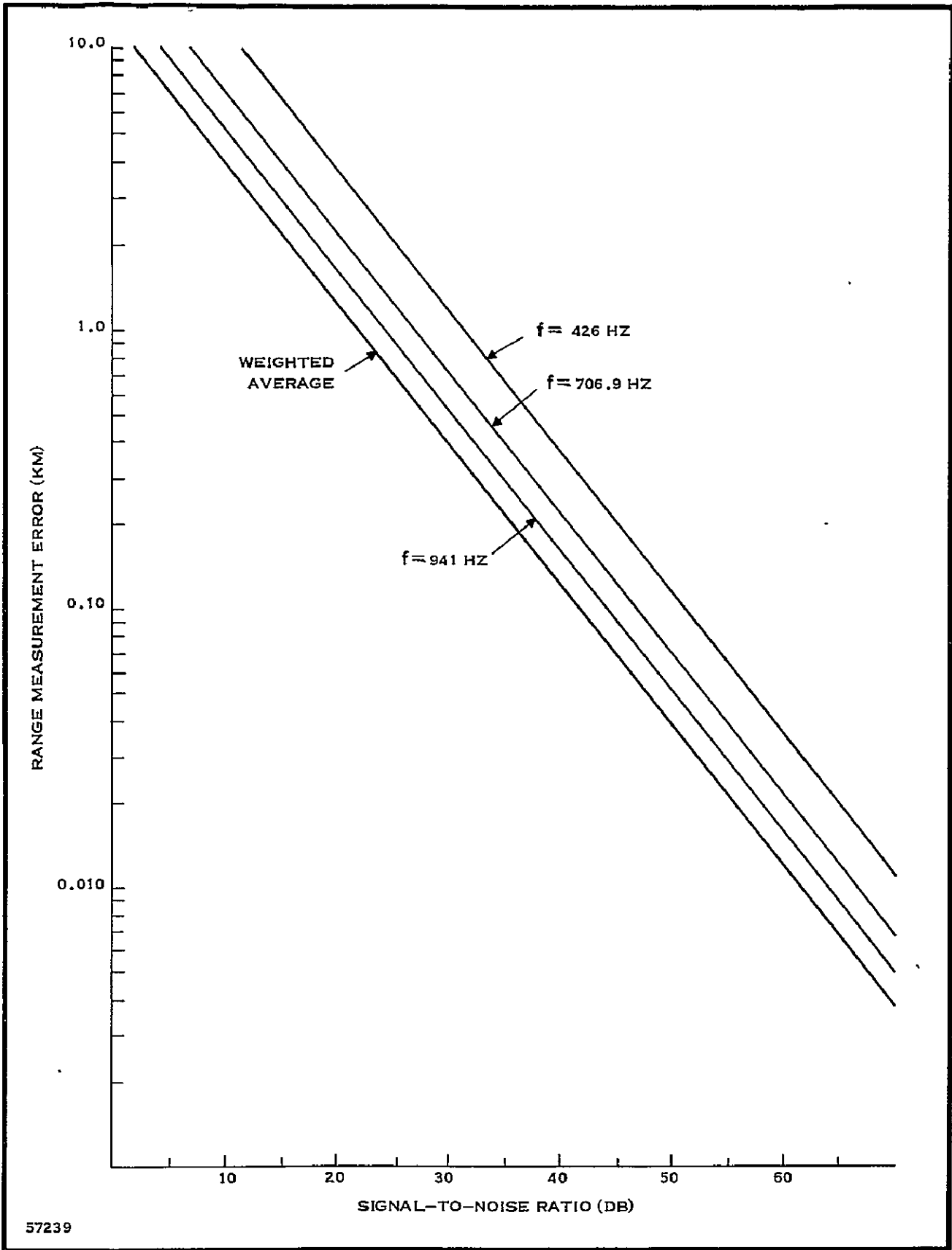


Figure 4-2. RMS Range Error Due to Phase Error as a Function of SNR

4.2 Range Ambiguity

For each phase measurement made at the GCC on the returned sidetones, there exists a range ambiguity due to an unknown number of integral cycles associated with the total path length. Therefore, each of the range measurements made at the three sidetone frequencies has a systematic ambiguity. This range ambiguity can be resolved in this sidetone ranging system by off-line digital processing. This involves combining multiples of the measured phase values to produce a set of calculated phase values which correspond to synthesized sidetones at lower frequencies. A sufficiently low sidetone frequency is used such that the range can be defined unambiguously within the constraints of satellite/aircraft geometry. Once the unambiguous phase value is calculated, a "walk-up" method is used to sequentially resolve the ambiguity of each phase estimate, or measurement, at the next higher sidetone frequency.

The frequencies of the sidetones generated at the GCC are 426.4 Hz, 706.9 Hz, and 941.4 Hz, and a phase measurement (ambiguous in the number of integral cycles) is made at each sidetone frequency. These phase measurements can be combined by means of off-line processing to produce calculated phase values at other frequencies because the frequencies of the generated sidetones are non-harmonically related. One such set of synthesized frequencies (which will be used in this experiment) is calculated from the following combinations of the measured sidetone phase values:

$$234.5 \text{ Hz} = [941.4 - 706.9] \text{ Hz}$$

$$145.9 \text{ Hz} = [2(426.4) - 706.9] \text{ Hz}$$

$$88.6 \text{ Hz} = [941.4 - 2(426.4)] \text{ Hz}$$

$$46.0 \text{ Hz} = [2(706.9) - 941.4 - 426.4] \text{ Hz}$$

$$31.3 \text{ Hz} = [2(941.4) + 706.9 - 6(426.4)] \text{ Hz}$$

$$14.7 \text{ Hz} = [706.9 - 3(941.4) + 5(426.4)] \text{ Hz}$$

The lowest synthesized tone of 14.7 Hz can be used to define a range unambiguously up to a path length of 20,000 Km, which is more than sufficient for resolving the unknown portion of the range over the various measurement paths in this experiment. The maximum unknown range value (approximately twice the Earth's radius, or 12,756 Km) occurs in the two-way path between the ATS-3 satellite and the aircraft terminal.

Because the range resolution capability of the 14.7-Hz tone is limited, a "walk-up" method is applied to sequentially resolve the ambiguity in the synthesized tones while proceeding to the ultimate range resolution provided by the three basic tones. The probability of incorrect ambiguity resolution as a function of signal-to-noise ratio of the generated tones is shown in Figure 4-3 for the three lowest synthesized tone values of 46.0 Hz, 31.3 Hz, and 14.7 Hz. The significance of the three lower-frequency tones is that the 31.3-Hz tone can be used to resolve range ambiguity over 84 percent of the possible path range with 5 dB less signal amplitude than the 14.7-Hz tone for equal performance. Similarly, the 46.0-Hz tone can be used to resolve ambiguity over 57 percent of the range and thus reduces the signal amplitude requirement another 4.5 dB. Other methods of resolving the total ambiguity would have to be applied with either of these higher-frequency tones; however, in many cases this would not be difficult because the 46.0-Hz tone would provide a minimum value of range ambiguity of 5,000 Km along the Earth's surface.

Some improvement in the probability of correctly resolving range ambiguities could be realized by adjusting the relative amplitudes of the three transmitted tones; however, this is not proposed in this experiment because it would require additional modification to the OPLE Control Center.

4.3 VHF Link Considerations

The VHF links that must be considered in the power budget analysis for this VHF ranging experiment are listed below in order of increasing signal-to-noise ratio:

- (1) The link from the GCC to the aircraft and return via the ATS-3 satellite
- (2) The link from the GCC to the aircraft via the ATS-3 satellite and return via the ATS-1 satellite
- (3) The link from the GCC to the ATS-3 satellite and return
- (4) The link from the GCC to the ATS-1 satellite and return.

This order is dependent upon the fact that both the ATS-1 and the ATS-3 are in full view of the aircraft and the GCC. In fact, the ATS-1 suffers an additional signal attenuation of the GCC due to its low elevation angle (3°); this degradation is approximately 5 dB. However, a higher-gain VHF antenna (18 dB rather than 13 dB) will be used for the ATS-1 receiver at the GCC. The return from the aircraft via the ATS-3 satellite has the least margin because the ATS-3 satellite transponder must relay a greater number of signals than the ATS-1 satellite transponder.

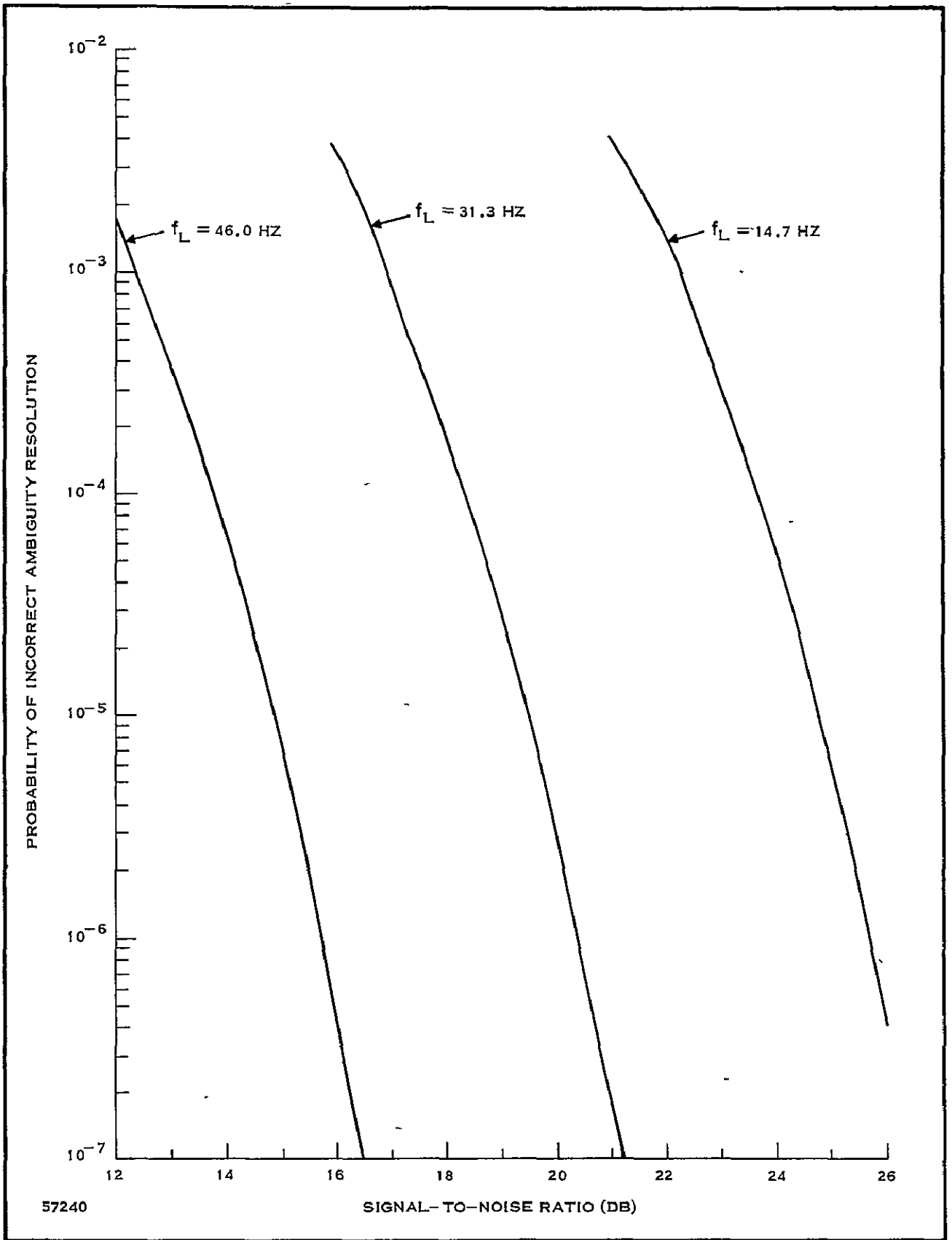


Figure 4-3. Ambiguity Resolution Versus Phase Noise

In the link analysis presented in the following paragraphs, optimum power sharing of the ATS-3 satellite power is first computed to maximize the performance of link (1). The performance of the other three links is then computed based upon these parameters. The worst-case analysis is then made without any power readjustment.

4.3.1 Optimum Ratio of GCC Power to Aircraft Transmitter Power

In this section, the ATS-3 satellite power sharing is determined so as to minimize the total noise power density that is added to the ranging tones when they are relayed from the GCC to the aircraft and back via the ATS-3 satellite. This optimization is accomplished by noting the following facts:

- (1) The satellite is power limited (P_s watts), and this power must be shared between (a) the tones relayed from the GCC to the aircraft (P_{sa} watts in 4 tones), (b) the pilot tone relayed from the GCC to the aircraft (P_j watts); (c) the ranging tones and aircraft receiver noise relayed from the aircraft to the GCC ($P_{sg} + P_{sgn}$ watts); and (d) the satellite noise that is not suppressed due to the sum of signals a, b, and c (P_w watts). It will be shown that P_w is negligible, and hence the power summation is:

$$P_s = P_{sa} + P_{sg} + P_{sgn} + P_j .$$

The reradiated aircraft receiver noise (P_{sgn}) is due to the aircraft transponder not being completely captured by the received ranging tones from the ATS-3 satellite. This power term can be kept arbitrarily small by a more complex terminal transponder design. For the conventional single-IF tone filter proposed for the transponder, however, this term may not be negligible. The ratio of the noise term (P_{sgn}) to the signal term (P_{sg}) is determined by the signal-to-noise ratio in the aircraft terminal transponder and hence,

$$P_{sg} + P_{sgn} = P_{sg} \left[1 + \frac{N_a B_a}{P_{sa} L_{as}} \right]$$

where N_a = noise power density in the terminal transponder receiver

B_a = terminal transponder tone filter bandwidth

L_{as} = link loss between aircraft and satellite.

	Nominal	Worst Case	Units
Satellite Transmitter			
Coupling Loss	-1.8		dB
Antenna Gain	8.5		dB
Path Loss	-167.0	-168.1	dB
Polarization Loss	-3	-4	dB
Multipath Loss	0	-4	dB
Aircraft Receiver			
Antenna Gain	2	0	dB
Coupling Loss	-2		dB
Link Loss	-163.3	-171.4	dB
Antenna Temperature	1000	1600	°K
Receiver Noise Figure	3	4	dB
Effective Receiver Temperature	1300		°K
Receiver Noise Power Density	-197.5	-195.5	dBw/Hz
Receiver Noise Power Density	-34.2	-24.1	dBw/Hz
	3.8×10^{-4}	3.9×10^{-3}	watts/Hz

Figure 4-4. Noise Power Density/Link Loss (N_a/L_{as})—Satellite to Aircraft
(Frequency = 135.6 MHz)

Using the nominal value for N_a/L_{as} (from Figure 4-4) of 3.8×10^{-4} watts/Hz, an IF bandwidth of 4 kHz, and an estimated P_{sa} of approximately 10 watts, the nominal value of P_{sgn} is negligible. Hence, the satellite power summation for nominal conditions becomes:

$$P_s - P_j = P_{sa} + P_{sg}$$

- (2) The contribution to the total noise by the GCC-to-satellite and aircraft-to-satellite links can be kept arbitrarily small by increasing the GCC and aircraft transmitter powers. Hence, the ratios of total noise power density

to signal power for the four ranging tones received at the GCC can be written as:

$$\frac{N}{P} = \frac{N_g}{P_{sg}L_{gs}} + \frac{N_a}{P_{sa}L_{as}}$$

where N_g = noise power density in the GCC receiver,

L_{gs} = link loss between the GCC and the satellite.

The other terms have been previously defined. Substituting for P_{sg} from item (1), differentiating with respect to P_{sa} , and solving the resulting quadratic equation for that value of P_{sa} giving the minimum value of N/P , gives:

$$P_{sa} = (P_s - P_j) \left[\frac{1 - \left(\frac{N_g L_{as}}{L_{sg} N_a} \right)^{1/2}}{1 - \frac{N_g L_{as}}{L_{sg} N_a}} \right]$$

It has been observed in OPLE tests with the ATS-3 satellite that the pilot tone must acquire approximately 25 percent of the total satellite power to achieve reliable operation. For $P_s = 40$ watts and using the nominal N/L ratios calculated in Figures 4-4 and 4-5, the optimum value of P_{sa} is:

$$P_{sa} = 22 \text{ watts}$$

$$\text{and } P_{sg} = 8 \text{ watts.}$$

- (3) Because the relative GCC and aircraft transmitter power levels control the satellite power sharing, the following equation can be written, subject to the assumption made in items (1) and (2):

$$\frac{L_{gs} P_g}{P_{sa}} = \frac{L_{as} P_a}{P_{sg}}$$

or

$$\frac{P_g}{P_a} = \frac{L_{as}}{P_{sg}} \frac{P_{sa}}{L_{gs}}$$

	Nominal	Worst Case	Units
Satellite Transmitter			
Coupling Loss	-1.8		dB
Antenna Gain	8.5		dB
Path Loss	-167.0	-168.1	dB
Polarization Loss	-3	-4	dB
Ground Receiver			
Antenna Gain	13		dB
Coupling Loss	-2.5		dB
Link Loss	-152.8	-154.9	dB
Antenna Temperature	1300	1600	°K
Receiver Noise Figure	3	4	dB
Effective Receiver Temperature	1600	2050	°K
Receiver Noise Power Density	-196.6	-195.5	dBw/Hz
Receiver Noise Power Density/Link Loss	-43.8	-40.6	dBw/Hz
	4.17×10^{-5}	8.7×10^{-5}	watts/Hz

Figure 4-5. Noise Power Density/Link Loss (N_g/L_{sg})—Satellite to Ground (Frequency = 135.6 MHz)

where P_g = GCC transmitter power in the tones
 P_a = aircraft transponder power.

Again, substituting nominal values:

$$\frac{P_g}{P_a} = 0.25.$$

Hence, if P_a is chosen to be 100 watts, P_g is 25 watts. This is well within the capabilities of the present OCC transmitter.

4.3.2 Link Power Budgets

In the previous section, the optimum satellite power division and GCC and aircraft transmitter power levels were calculated by making a number of simplifying assumptions. In this section, the actual nominal and worst-case ratios of noise power density to signal power per ranging tone are calculated for the various ranging paths, using information presented in Reference 7. First, the following accurate results are required. Using the derivation in item (2) of the last section, but not making the simplifying assumptions used in that section:

$$P_{sa} = \frac{P_s - P_j}{1 + \frac{L_{as} P_a}{L_{gs} P_g}} \cdot$$

Using the exact result for item (3) in the last section:

$$P_{sg} = \frac{L_{as} P_a P_{sa}}{L_{gs} P_g \left[1 + \frac{N_a B_a}{P_{sa} L_{as}} \right]} \cdot$$

The nominal values, using $B_a = 4$ kHz and the results of Figures 4-4 and 4-5, are:

$$P_{sa} = 22 \text{ watts}$$

$$P_{sg} = 8 \text{ watts.}$$

The worst-case values, using the results in the same figures, are:

$$P_{sa} = 27.6 \text{ watts}$$

$$P_{sg} = 1.56 \text{ watts.}$$

4.3.2.1 Link from GCC to Aircraft and Back Via ATS-3 Satellite

The effective noise power ratio per ranging tone is given by:

$$\left[\frac{N}{P} \right]_1 = 4 \left[\frac{N_g}{P_{sg} L_{gs}} + \frac{N_s}{P_a L_{as}} \left(1 + \frac{N_a B_a}{P_{sa} L_{as}} \right) + \frac{N_a}{P_{sa} L_{as}} + \frac{N_s}{P_g L_{gs}} \right] \cdot$$

Inserting nominal values from Figures 4-4 through 4-7 gives:

$$\left[\frac{N}{P} \right]_1 = 1.2 \times 10^{-4} \text{ per Hz, or } -39.2 \text{ dB/Hz.}$$

	Nominal	Worst Case	Units
Aircraft Transmitter			
Coupling Loss	-2		dB
Antenna Gain	2	0	dB
Path Loss	-168.5	-169.7	dB
Polarization Loss	-3	-4	dB
Multipath Loss	0	-4	dB
Satellite Receiver			
Antenna Gain	8		dB
Coupling Losses	-1.8		dB
Link Loss	-165.3	-173.5	dB
Antenna Temperature	800.		°K
Receiver Noise Temperature	400	1200	°K
Effective Receiver Temperature	1200	2000	°K
Receiver Noise Power Density	-197.8	-195.5	dBw/Hz
Receiver Noise Power Density/Link Loss	-32.5	-22	dBw/Hz
	5.6×10^{-4}	6.3×10^{-3}	watts/Hz

Figure 4-6. Noise Power Density/Link Loss (N_s/L_{as})—Aircraft to Satellite
(Frequency = 149.2 MHz)

Using simultaneous worst-case values, however:

$$\left[\frac{N}{P} \right]_1 = 1.2 \times 10^{-3} \text{ per Hz, or } -29.2 \text{ dB/Hz.}$$

4.3.2.2 Link from GCC to Aircraft Via ATS-3 Satellite and Return Via ATS-1 Satellite

This link will have slightly less margin than the link described in Paragraph 4.3.2.1

	Nominal	Worst Case	Units
GCC Transmitter			
Coupling Loss	-2.5		dB
Antenna Gain	13		dB
Path Loss	-168.5	-169.7	dB
Polarization Loss	-3	-4	dB
Satellite Receiver			
Antenna Gain	8		dB
Coupling Losses	-1.8		dB
Link Loss	-154.8	-157.0	dB
Antenna Temperature	800		°K
Receiver Noise Temperature	400	1200	°K
Effective Receiver Temperature	1200	2000	°K
Receiver Noise Power Density	-197.8	-195.5	dBw/Hz
Receiver Noise Power Density/Link Loss	-43	-38.5	dBw/Hz
	5×10^{-5}	1.4×10^{-4}	watts/Hz

Figure 4-7. Noise Power Density/Link Loss (N_s/L_{gs})—GCC to Satellite
(Frequency = 149.2 MHz)

4.3.2.3 Link from GCC to ATS-3 Satellite and Return

The effective noise power ratio per ranging tone is:

$$\left[\frac{N}{P}\right]_3 = 4 \left[\frac{N_g}{P_{sg} L_{gs}} + \frac{N_s}{P_g L_{gs}} \right].$$

Inserting nominal values gives:

$$\left[\frac{N}{P}\right]_3 = 2.9 \times 10^{-5} \text{ per Hz, or } -45.4 \text{ dB/Hz.}$$

Worst-case values give:

$$\left[\frac{N}{P}\right]_3 = 2.2 \times 10^{-4} \text{ per Hz, or } -36.5 \text{ dB/Hz.}$$

4.3.2.4 Link from GGC to ATS-1 Satellite and Return

This link will have slightly less margin than the link described in Paragraph 4.3.2.3.

4.3.3 Channel Allocations

The factors to be considered in determining the channel allocations for this experiment are

- (1) An interfering signal has been noted in the ATS-3 satellite output at approximately channel 28 frequency
- (2) The GGC self-check tones are transmitted in channel 21
- (3) The ATS-3 pilot tone will be transmitted in channel 12
- (4) It is preferable not to allocate the terminal transponders any existing OPLE PEP channels.

Hence, suitable transmit channels for the terminal transponders are OPLE channels 16 and 34.

4.3.4 Radio Frequency Interference

A factor which must be considered in the VHF ranging experiment is that of radio frequency interference (RFI). Presumably, the system will not be purposely jammed, however, the VHF band employed by the experiment will be shared with other users. Because of the very narrow post detector bandwidth at the Ground Control Center, it is unlikely that RFI will appreciably affect the phase measuring circuitry. On the other hand, a strong interference signal at or near the pilot tone or A/R tone frequency could result in loss of phase-lock, either at the aircraft terminal or the Ground Control Center. However, such an interference signal can be detected at the GGC by means of the satellite monitoring circuitry.

Because of the heavy use of the VHF band of interest by commercial air traffic, it is highly probable that interference problems will be encountered during the performance of the VHF Satellite Navigation Experiment. In this event, two alternatives exist. First, the GGC and terminal transponders could be modified to permit reallocation of channels and thus place the interference signal in an unused channel. Second, the experiment could be rescheduled for periods of minimum interference.

4.4 Ionospheric Compensation

The VHF range estimates used in this experiment contain significant bias errors due to the ionosphere. In the following sections,

the magnitude of this bias error and a method for introducing a bias correction term are discussed.

4.4.1 The Need for Ionospheric Compensation

The estimate of the range between the aircraft and a satellite contains a bias error due to the ionosphere and the troposphere. The magnitude of these bias terms is shown in Figures 4-8 (Reference 2) and 4-9. The tropospheric bias is independent of frequency but is a function of the temperature of the troposphere, the total pressure, and the partial pressure of the water vapor. Even when these quantities vary widely the tropospheric bias does not depart significantly from the curve in Figure 4-8. Hence, if the elevation angle of the aircraft to the satellite is known, or even roughly known, a correction factor can be obtained from Figure 4-8 to remove the tropospheric bias. This correction is of a small magnitude (35 meters and 3 m3534s for 3° and 37° elevation angles, respectively) and can be made with a high degree of accuracy.

On the other hand, the ionospheric bias is shown in Figure 4-9 to be of significant magnitude and therefore deserves closer attention. For example, daytime values of integrated electron density typically vary between 2×10^{17} and 6 or 8×10^{17} electrons/m²; hence, the ionospheric bias is as large as 1.5 Km to 5 Km for 3° elevation angles. When the elevation angle increases to 37°, the bias is still considerable (0.6 Km to 2.5 Km). During periods of increased sunspot activity, the integrated electron density sometimes exceeds 1×10^{18} electrons/m². In this worst-case condition, the bias becomes as large as 8 Km. Needless to say, some method is needed to remove this bias from the range estimate. Various possibilities of doing this are discussed in the next paragraph.

4.4.2 Possible Methods of Ionospheric Compensation

The methods for measuring or estimating the ionospheric bias may be classified as direct and indirect measurements. The former measures the ionospheric bias by taking the difference between biased and unbiased range estimates while the latter measures the integrated electron density to determine the ionospheric bias.

4.4.2.1 Direct Ionospheric Bias Measurements

This measurement is made by taking the difference between biased and unbiased range estimates of the distance between the Ground Control Center and the ATS-3 satellite. The difference between the two measurements is attributed to ionospheric bias. Of course, careful consideration must be given to equipment calibration and accuracy to insure that other effects do not add to the ionospheric bias.

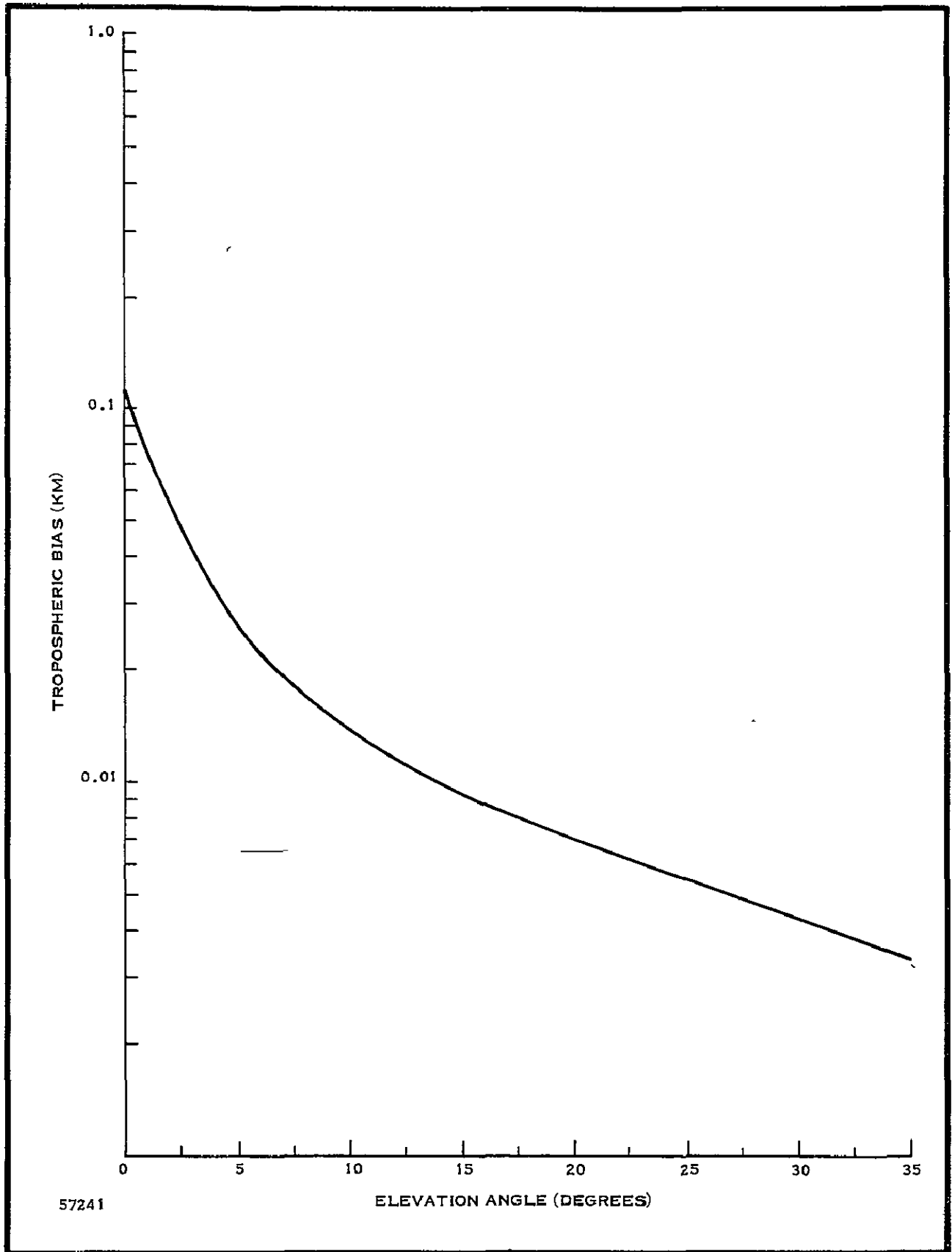


Figure 4-8. Tropospheric Bias Versus Elevation Angle

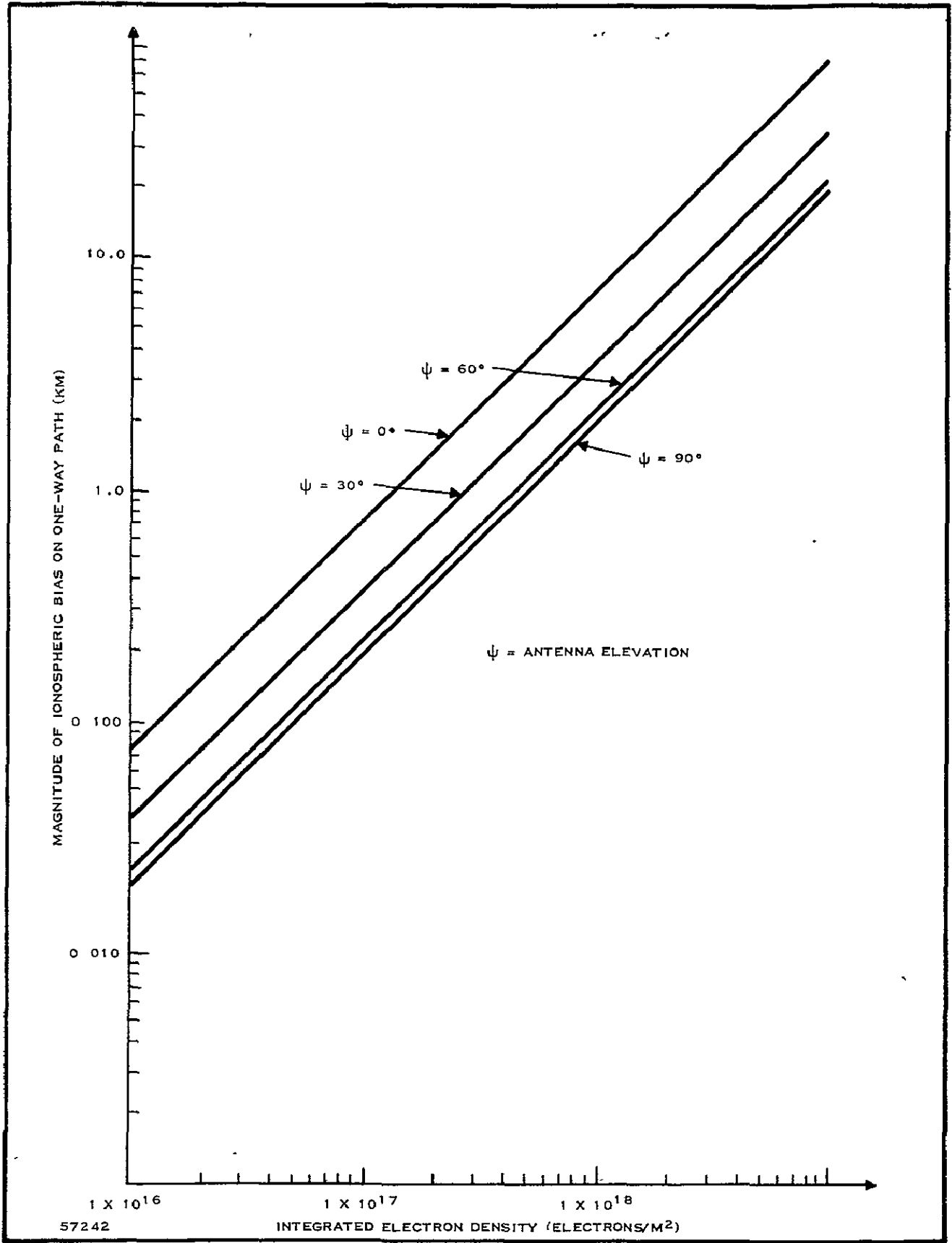


Figure 4-9. Magnitude of Ionospheric Bias Term as a Function of Integrated Electron Density

The first of two direct bias measurements uses range estimates made at VHF and SHF. Because the ionospheric bias decreases as the square of the frequency, the bias remaining in a range estimate made at 4.5 GHz would be $1/900^{\text{th}}$ as large as the bias in the VHF measurement at 149.22 MHz. This reduces the bias to a few meters which can be neglected when compared to bias of several kilometers in the VHF range estimate. The advantage of this method is that it gives an accurate result, the accuracy being related to the SHF frequency. It suffers the disadvantage of requiring a measurement by other equipment (i. e., SHF equipment) which is not an integral part of the Ground Control Center.

The second method for direct bias measurements uses VHF range estimates of the ground station/satellite distance made during the night and at the moment of interest. Between midnight and two a. m. local time, the ionospheric bias reaches its minimum because of the nighttime reduction in ionization of the ionosphere. Hence, a VHF range estimate made during these hours will have a minimum bias compared to those made of other hours of the day. Typical night values of integrated electron density are 3 to 6×10^{16} electrons/ m^2 which correspond to biases of 100 to 350 meters (for elevation angles from 3° to 37°). Assuming that the true range to the satellite does not vary over several nights (a good assumption), the minimum of several nighttime range estimates could be used as the reference. This reference is then subtracted from the satellite range estimate made at the moment of interest. The difference, although less accurate than the first method, is an indication of the ionospheric bias along the ground station/satellite path. However, the easy availability of the reference measurement at night makes this approach very attractive. Therefore, because of its reasonable accuracy and easy implementation, this second method of measuring the ionospheric bias is the approach to be taken in this experiment.

4.4.2.2 Indirect Ionospheric Bias Measurements (Faraday Rotation)

It is well known that the angle through which a polarized wave is rotated in traversing the satellite/ground station path is directly proportional to the integrated electron density of the ionosphere. Hence, by measuring the angle of polarization of the received wave at the ground station, the ionospheric bias can be determined. However, this method has the disadvantage of requiring the use of supplementary antennas and receivers to make the Faraday rotation measurement. The need for additional equipment makes this approach unattractive from the viewpoint of the present experiment.

4.4.3 Correlation Between Measured Ionospheric Bias and Predicted Ionospheric Bias

The ionospheric bias is measured for the ground station/satellite link in all the cases discussed above. However, the range estimate of the satellite/aircraft distance requires that the ionospheric bias be known for that link also (see Appendix B). Therefore, the important question is how does the ionospheric bias at one location relate to that at another location. There is extensive research being conducted on this problem by Dr. Aldo da Rosa of Stanford University. The desired result of his work is a quantitative relationship between the integrated electron density at two different locations. The important parameters in this relation are the time of day, latitude, temperature profile of the ionosphere, and transition height between oxygen and hydrogen molecules in the atmosphere. Dr. da Rosa has made daily measurements of the integrated electron density at points separated by a few hundred kilometers and at points separated by several thousand kilometers. Insufficient data is available to really test his model thoroughly.

In the meantime, some preliminary observations can be made regarding the variation of the integrated electron density as a function of location. The principle variation is a latitude effect. This latitude effect is closely associated with the variation in the F₂ layer electron concentration as a function of latitude. J. O. Thomas (Reference 3) has studied this variation with latitude and has plotted the variation as a function of magnetic dip angle for several months through the fall and winter of 1957 (see Figure 4-10). Figure 4-11 shows how the median of this latitude effect varies over a day in December 1957. Because these curves are plotted as a function of magnetic dip angle, one must know the magnetic dip angles for the locations of interest.

Figures 4-12 (Reference 4) and 4-13 (Reference 5) show the diurnal variations in integrated electron density at Hawaii/Stanford and Stanford/Ely, Nevada. The Hawaii/Stanford data was taken from Syncom III in 1964 while the Stanford/Ely data is more recent and was obtained from the ATS-1 satellite. The magnetic dip angles for Stanford and Ely are 63° N and 64° N, respectively. From Figure 4-10, the latitude effect between these two points is seen to be negligible as borne out by the close correspondence of the curves in Figure 4-13. Hence, for locations which are within a few hundred kilometers of one another, the integrated electron densities are essentially identical. Dr. da Rosa has much more Stanford/Ely data to substantiate this result.

However, Stanford and Hawaii have magnetic dip angles of 63° and 40°, respectively. This results in a significant difference in the levels of integrated electron densities over the measured paths because of the latitude difference between the two locations.

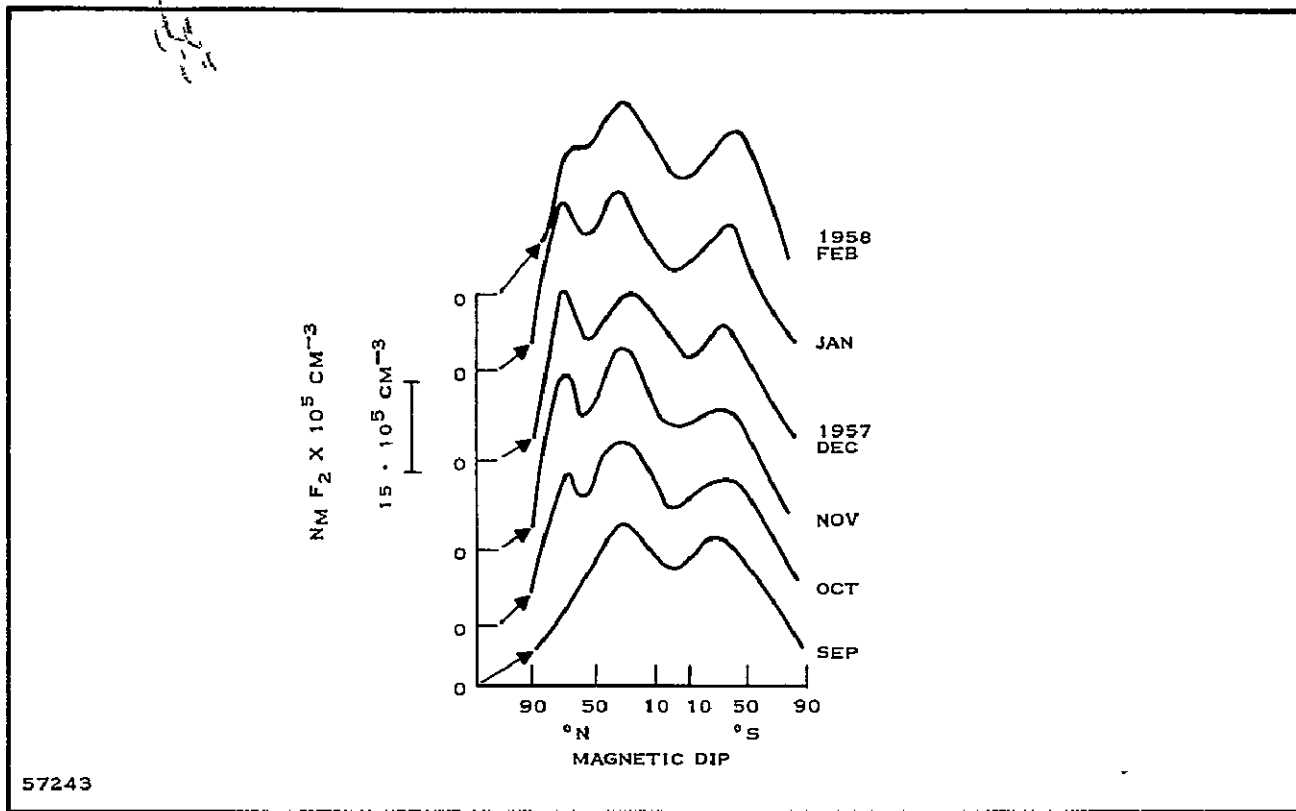


Figure 4-10. The Variation with Magnetic Dip of the Monthly Median Local Noon Values of $N_m F_2$ for Different Months

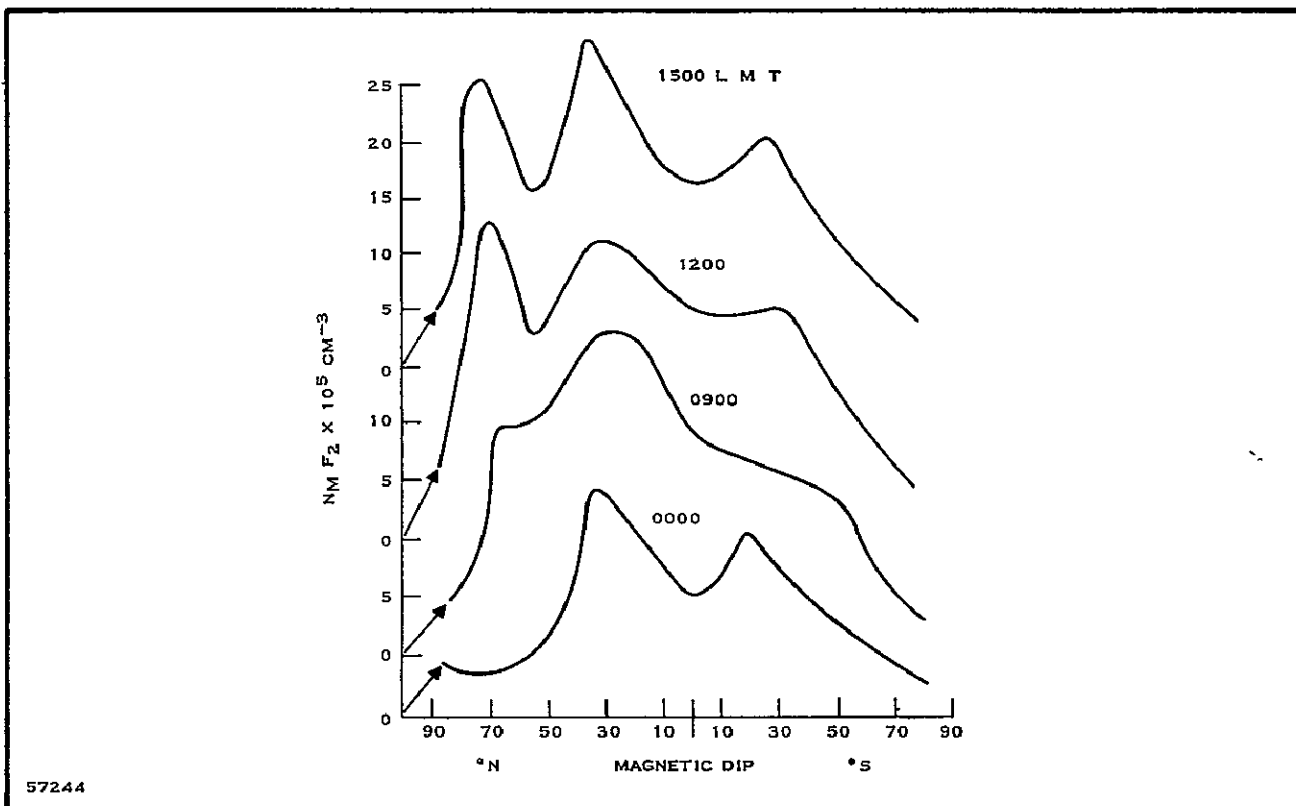


Figure 4-11. The Variation with Magnetic Dip of the Monthly Median Values of $N_m F_2$ at Different Hours of the Day in December 1957

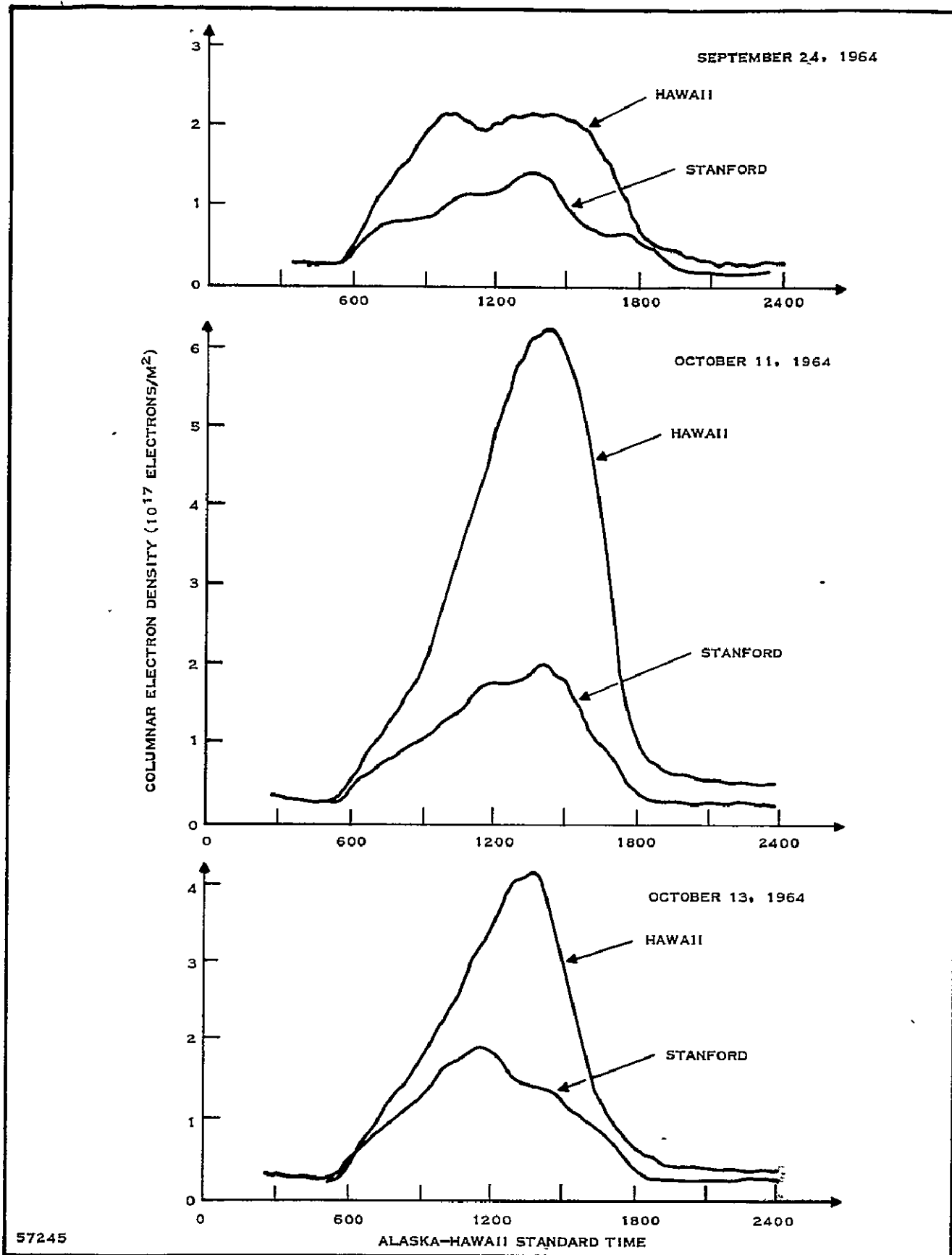
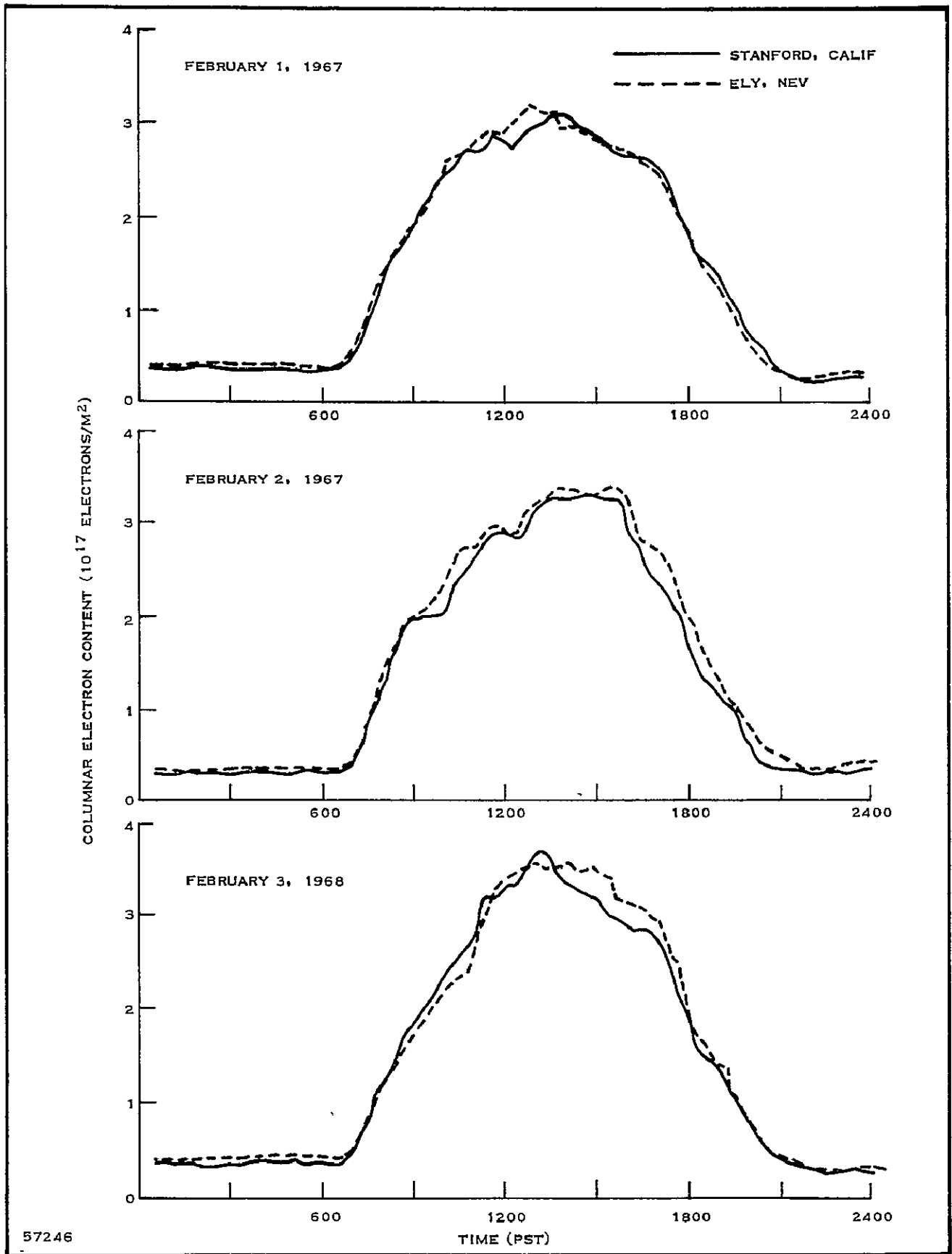


Figure 4-12. Comparison of Columnar Electron Content Versus Time Curves Obtained from Syncom III at Hawaii and Stanford (The Stanford Curve is Shifted to the Right to Correspond to Local Time at Hawaii)



57246

Figure 4-13. Comparison of Columnar Electron Content Versus Time Curves Obtained from ATS-1 at Ely and Stanford. (The Ely curve is shifted approximately one-half hour to the right to correspond to local time at Stanford.)

The 1957 data in Figure 4-10 indicate that the Hawaii levels should be 1.58 and 1.38 times the Stanford data in September and October, respectively. These figures should be closer to 2 and 2.5 to more nearly relate the data in Figure 4-12. At the moment, the latitude effect curves for the appropriate days in September and October 1964 are not available. However, Dr. da Rosa expects to have prediction formulas available soon that will relate even more closely the Stanford/Hawaii observations (Reference 6). Therefore, for this experiment the ionospheric bias as measured at the Ground Control Center will be used together with appropriate elevation angle and latitude effects to correct the aircraft/satellite range estimates.

4.5 Velocity Considerations

The major effect of aircraft velocity is to shift the carrier tone frequency received by the GCC. Because this carrier tone is tracked by phase-lock loops in the GCC, the doppler shift frequency must be limited to the error frequency tracking range of the phase-lock loops. This has been demonstrated to be greater than ± 300 Hz. Therefore, the maximum allowable aircraft velocity in this experiment is 1170 knots, a value which produces a frequency shift of 300 Hz on the transmitted 149.2-MHz carrier. This value is set assuming that all other carrier frequency errors are compensated for in the GCC through calibration settings of the two VHF receiver synthesizers, one for each satellite. The allowable doppler shift frequency range could be expanded by redesign of the phase-lock loops in the GCC.

5.0 POSITION LOCATION

There exist several coordinate systems, each with their own set of equations describing the satellites and aircraft geometry, which can be used in discussing the position location of the aircraft terminal. However, there is one set of coordinates with its associated equations that is most convenient in the sense that the equations can be solved in a straightforward manner. This is the set of orthogonal earth centered coordinates together with radius vectors defined in terms of direction cosines. It is the purpose of this section to discuss the static geometry of this position location experiment.

The geometrical relation between the satellites and the aircraft terminal is shown in Figure 5-1. The Ground Control Center is not shown because it does not enter directly into the position location geometry. However, it does enter into the earlier stage of measuring the ranges R_1 and R_3 . See Figure B-1 and Appendix B for the way in which R_1 and R_3 are estimated from the sidetone phase measurements.

In this experiment, the satellite locations are assumed to be known. A precise statement of the problem is

GIVEN $\underline{R}_{01} = R_{01} \underline{b}_1$ = vector from center of the Earth to the ATS-1 satellite

$\underline{R}_{03} = R_{03} \underline{b}_3$ = vector from center of the Earth to the ATS-3 satellite

where

$\underline{b}_1^T = (b_{11}, b_{12}, b_{13})$ is a vector whose elements are the direction cosines for the ATS-1 satellite, and \underline{b}_3 is the similar vector for the ATS-3 satellite.

MEASURED R_1 = range between the ATS-1 satellite and the aircraft terminal

R_3 = range between the ATS-3 satellite and the aircraft terminal

R_h = range between Earth's center and the aircraft terminal.

ESTIMATE: $R_h \underline{b}_a$ = the position vector of the aircraft terminal

$\underline{b}_a^T = (b_{a1}, b_{a2}, b_{a3})$ = the direction cosine vector for the aircraft terminal.

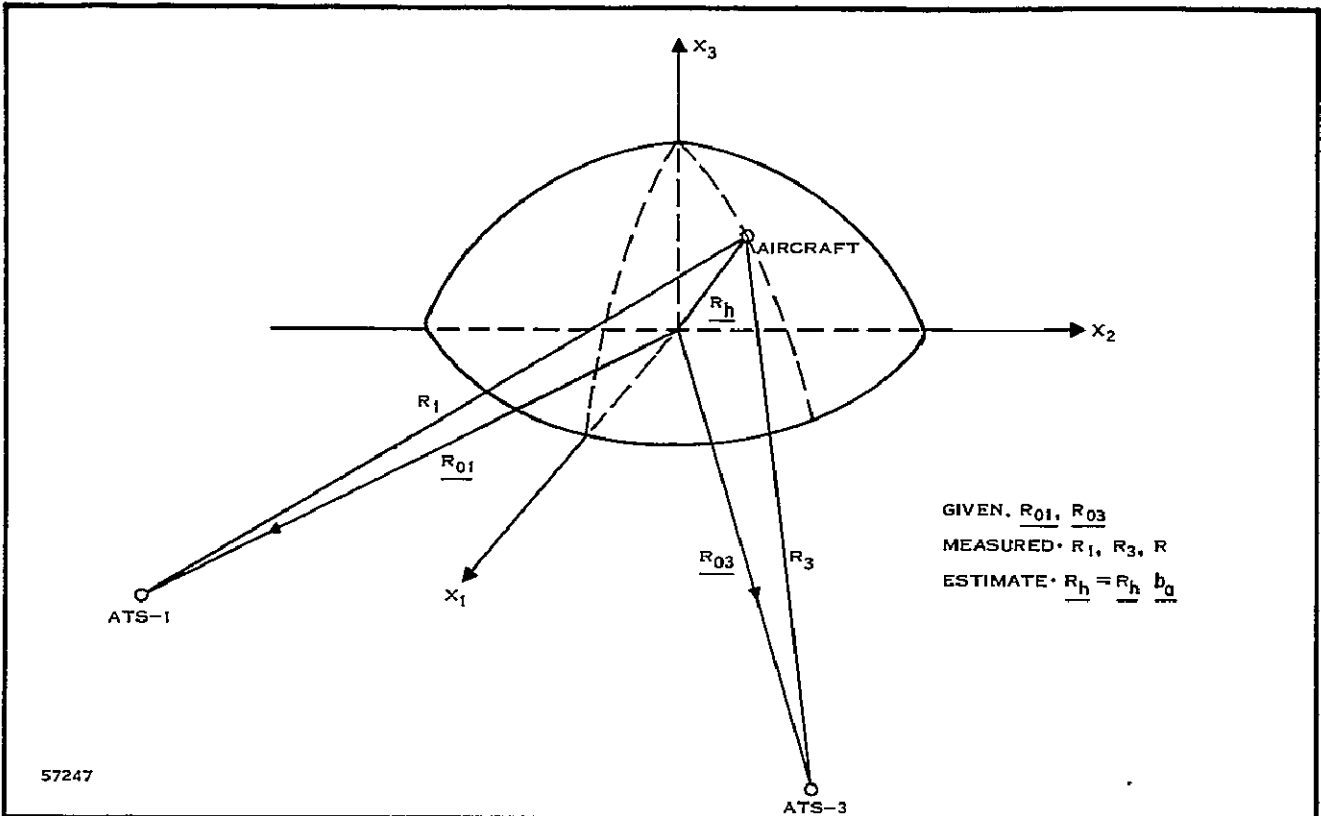


Figure 5-1. Geometrical Relation Between the Earth, Satellites, and Aircraft Terminal

The unknown is \underline{b}_a , a three-component vector. To determine these components, three independent equations are required. The law of cosines yields two equations which are

$$R_1^2 = R_{01}^2 + R_h^2 - 2R_{01}R_h \underline{b}_a^T \underline{b}_1 \quad (5-1)$$

$$R_3^2 = R_{03}^2 + R_h^2 + \underline{R_h}^2 - 2R_{03}R_h \underline{b}_a^T \underline{b}_3. \quad (5-2)$$

The third equation is the auxiliary equation for the direction cosines:

$$b_{a1}^2 + b_{a2}^2 + b_{a3}^2 = 1. \quad (5-3)$$

Equations (5-1) and (5-2) yield:

$$\underline{b}_a^T \underline{b}_1 = b_{11}b_{a1} + b_{12}b_{a2} + b_{13}b_{a3} = \frac{R_{01}^2 + R_h^2 - R_1^2}{2R_{01}R_h} = D_1 \quad (5-4)$$

$$\underline{b}_a^T \underline{b}_3 = b_{31}b_{a1} + b_{32}b_{a2} + b_{33}b_{a3} = \frac{R_{03}^2 + R_h^2 - R_3^2}{2R_{03}R_h} = D_3. \quad (5-5)$$

The three independent equations to be solved for the direction cosines of the aircraft terminal are (5-3), (5-4) and (5-5). However, the non-linear equation in (5-3) complicates the solution somewhat.

The present satellite positions are approximately

ATS-1 155° W longitude, 0° latitude
 ATS-3 75° W longitude; 0° latitude.

The satellites are in an orbital plane that is inclined 0.3° to the equatorial plane. The uncertainty in the positions of the satellites is ±2 Km with the maximum of the error ellipse perpendicular to the orbital plane. As pictured in Figure 5-1, longitude is measured from the X₂ axis toward the X₁ axis. The direction cosines are measured from each of the three orthogonal axes to the vector in question. For example, b_{a1} is the cosine of the angle between the X₁ axis and the position vector R_h. Using this notation, vectors b₁ and b₃ are:

$$\underline{b}_1 = \begin{bmatrix} b_{11} \\ b_{12} \\ b_{13} \end{bmatrix} = \begin{bmatrix} \cos 65^\circ \\ \cos 15^\circ \\ \cos 90^\circ - \phi_1 \end{bmatrix} = \begin{bmatrix} 0.423 \\ -0.905 \\ \approx \phi_1 \end{bmatrix} \quad (5-6)$$

$$\underline{b}_3 = \begin{bmatrix} b_{31} \\ b_{32} \\ b_{33} \end{bmatrix} = \begin{bmatrix} \cos 15^\circ \\ \cos 75^\circ \\ \cos 90^\circ - \phi_3 \end{bmatrix} = \begin{bmatrix} 0.965 \\ 0.259 \\ \approx \phi_3 \end{bmatrix} \quad (5-7)$$

ϕ_1 and ϕ_3 are small angles which account for the fact that the orbital plane of the satellites is tilted a maximum of $(5.24 \pm 0.0475)(10^{-3})$ radians with respect to the Earth's equatorial plane. The error term represents the uncertainty in satellite position.

Because the angles ϕ_1 and ϕ_3 are small, they can be neglected on a first-cut at the solution. The steps involved in determining the position of the aircraft terminal from Equations (5-3) to (5-5) are

STEP 1: Assume $b_{13} = b_{33} = 0$

Equations (5-4) and (5-5) become:

$$b_{11}b_{a1} + b_{12}b_{a2} = D_1(R_1, R_h, R_{01}) \quad (5-8)$$

$$b_{31}b_{a1} + b_{32}b_{a2} = D_3(R_3, R_h, R_{03}) \quad (5-9)$$

from which

$$b_{a1} = \frac{b_{32}D_1 - b_{12}D_3}{\Delta} \quad (5-10)$$

$$b_{a2} = \frac{b_{11}D_3 - b_{31}D_1}{\Delta} \quad (5-11)$$

where

$$\Delta = b_{11} b_{32} - b_{31} b_{12}.$$

Also, from Equation (5-3):

$$b_{a3} = \pm \sqrt{1 - b_{a1}^2 - b_{a2}^2}. \quad (5-12)$$

STEP 2: The Transformations to Latitude and Longitude

$$\text{Latitude} = 90^\circ - \cos^{-1} b_{a3} \quad (5-13)$$

$$\text{Longitude} = \tan^{-1} \left(\frac{b_{a1}}{b_{a2}} \right). \quad (5-14)$$

STEP 3: Correction for Satellite Position

Solving Equation (5-4) for b_{a1} when $b_{13} \neq 0$ yields:

$$b'_{a1} = \frac{D_1 - b_{12}b_{a2}}{b_{11}} - \frac{b_{13}b_{a3}}{b_{11}} \quad (5-15)$$

$$b'_{a1} = b_{a1} - \left(\frac{b_{13}}{b_{11}} \right) b_{a3}$$

where b_{a1} and b_{a3} were previously defined in Equations (5-10) and (5-12). Likewise, solving Equation (5-5) for b_{a2} when $b_{33} \neq 0$ yields:

$$b'_{a2} = \frac{D_2 - b_{31}b_{a1}}{b_{32}} - \frac{b_{23}b_{a3}}{b_{32}}$$

$$b'_{a2} = b_{a2} - \left(\frac{b_{33}}{b_{32}} \right) b_{a3}. \quad (5-16)$$

The effect of considering the small angles ϕ_1 and ϕ_3 is to change the direction cosines. The third direction cosine is likewise affected:

$$\begin{aligned}
 b'_{a3} &= \pm \sqrt{1 - (b'_{a1})^2 - (b'_{a2})^2} \\
 &= \pm \left\{ 1 - b_{a1}^2 - b_{a2}^2 - \left[-2 \frac{b_{13}}{b_{11}} b_{a1} b_{a3} \right. \right. \\
 &\quad \left. \left. + \left(\frac{b_{13}}{b_{11}} b_{a3} \right)^2 \right] \right. \\
 &\quad \left. - \left[-2 \frac{b_{33}}{b_{32}} b_{a1} b_{a3} + \left(\frac{b_{33}}{b_{32}} b_{a3} \right)^2 \right] \right\}^{1/2}. \quad (5-17)
 \end{aligned}$$

The new latitude and longitude which result from the correction are obtained by using the new direction cosines in Equations (5-13) and (5-14).

STEP 4: Correction for Range Errors

Range errors ΔR_1 and ΔR_3 result in changes in D_1 and D_3

$$\Delta D_1 = \frac{R_1 \Delta R_1}{R_{01} R_h}, \text{ and } \Delta D_3 = \frac{R_3 \Delta R_3}{R_{03} R_h}. \quad (5-18)$$

These errors result in changes in the direction cosines as given by:

$$b''_{a1} = b_{a1} + \frac{b_{32} \Delta D_1 - b_{12} \Delta D_3}{\Delta} \quad (5-19)$$

$$b''_{a2} = b_{a2} + \frac{b_{11} \Delta D_3 - b_{31} \Delta D_1}{\Delta}. \quad (5-20)$$

This carries over to a change in b_{a3} and then into the final latitude and longitude of the aircraft terminal. These errors and their effects are examined in greater detail in Section 6.0.

6.0 ERROR ANALYSIS

Two types of errors are of primary importance in an error analysis of this experiment. Namely, they are the measurement errors and the final position location errors. The measurement errors refer to errors or uncertainties in the measured quantities which are used in the position location formulas of Section 5.0. These include the two aircraft/satellite ranges, R_1 and R_3 , the aircraft/Earth center range, R_h , and the satellite position. Sections 6.1, 6.2, and 6.3 discuss the sources of error and the magnitude of the error variance for each of the above cases.

The position location accuracy covered in Section 6.4 relates the errors in R_1 , R_3 , R_h , and satellite position to errors in the position location. The position location error is the important final consideration, but it is so closely related to the range errors and satellite position uncertainty that an error analysis is not complete without considering both aspects.

6.1 VHF Range Measurement Errors

In determining the aircraft's position, one must know the aircraft to ATS-1 and aircraft to ATS-3 range in addition to the aircraft altitude. These ranges are referred to as R_1 and R_3 , respectively (see Appendix B, Figure B-1). Because these ranges cannot be measured directly, they are estimated by appropriately combining several measurable ranges. The relationships are:

$$R_1 = R_{g3a1g} - 1/2(R_{g3a3g} + R_{g1g}) \quad (6.1-1)$$

$$R_3 = 1/2(R_{g3a3g} - R_{g3g}). \quad (6.1-2)$$

In terms of the sidetone phase delay measurements, the range estimates are:

$$\hat{R}_1 = \frac{\Delta f_{21}}{c} \left[\theta_{21g3a1g} - 1/2 \theta_{21g3a3g} - 1/2 \theta_{21g1g} \right] - \csc \psi_c \Delta s_{tropc} - \beta_2 \frac{b}{2} \alpha_c K_c \quad (6.1-3)$$

and

$$\hat{R}_3 = \frac{c}{2\Delta f_{21}} \left[\theta_{21g3a3g} - \theta_{21g3g} \right] - \csc \psi_B \Delta s_{tropB} - \beta_2 \alpha_B K_B \frac{b}{2} \quad (6.1-4)$$

The mean error in R_1 and R_3 is non-zero, resulting from non-zero means in the tropospheric and ionospheric bias correction terms. The mean square error in R_1 and R_3 is the sum of the mean square errors due to calibration, phase noise, ionospheric bias, and multipath under the assumption that each of these errors is independent. Our main interest is in the error variance, which is the difference between the mean square error and the square of the mean error. Because of the independence of the various errors, the error variances from each source add to form the total error variance for R_1 or R_3 .

In Sections 6.1.1 through 6.1.4, each of the error sources are discussed. There it will be seen that the ionospheric error variance dominates the other error variances. That is:

$$\begin{aligned} \text{var}(\Delta R_1) &= \text{var}(\text{calibration}) + \text{var}(\text{phase noise}) + \\ &\quad \text{var}(\text{ionosphere}) + \text{var}(\text{multipath}) \\ &\approx \text{var}(\text{ionosphere}) \end{aligned}$$

and $\text{var}(\Delta R_3) \approx \text{var}(\text{ionosphere})$.

Because the error variance due to the ionosphere is the same for either R_1 or R_3 , $\text{var}(\Delta R_1) \approx \text{var}(\Delta R_3)$. This result will simplify later portions of the error analysis.

6.1.1 Calibration Error

To compute a distance value in sidetone ranging, the portion of sidetone phase shift resulting from the delay of propagation through the transmission media must be separated from the phase shifts resulting from other sources. In this experiment, the effect of other sources of phase shift is removed by an off-line calibration process. Residual phase shift values not removed by calibration are defined as the system calibration error. If daily calibration runs are made, the expected one-sigma value of the system calibration error in the VHF range measurement is 0.3 Km. Major sources of phase shifts which are removed by calibration are the tone filters and phase detectors of the GCC, the filters in the satellite transponders, and the filters in the aircraft terminal.

The calibration procedure for this experiment is to connect the GCC directly to the ATS-3 VHF transponder simulator and record the resulting zero-range phase measurements. These phase measurements are the calibration values of phase shift which are subtracted from succeeding phase measurements in the off-line processing. Residual phase shift sources not removed by this calibration are the linearity of the phase detector and analog-to-digital converter in the GCC, quantizing error in the digital processing, and the sidetone phase shift difference between the ATS-3 satellite transponder and the satellite

transponder simulator. A similar calibration procedure with the ATS-1 VHF transponder simulator is required if the phase shifts of the side-tones through the ATS-1 satellite transponder are significantly different from the phase shifts through the ATS-3 satellite transponder.

The phase shift through the aircraft terminal is likewise calibrated by connecting it to the ATS-3 VHF transponder simulator. With this connection, the zero-range values in the link from the GCC to satellite to aircraft terminal and return are measured and used for calibration.

6.1.2 Phase Noise

Phase noise is that random noise component which is included with the sidetone signals at the VHF receiver output of the GCC. The resulting signal-to-noise ratio of the received sidetones is related to an RMS range error as shown in Figure 4-2. At the worst-case value of signal-to-noise ratio predicted for this experiment (30 dB within the 1-Hz processor bandwidth), the RMS value of VHF range measurement error due to phase noise is 0.4 Km.

Another consideration of phase noise is its effect on resolving the VHF range ambiguity. The probability of incorrect ambiguity resolution as a function of signal-to-noise ratio is shown in Figure 4-3. At the predicted worst-case signal-to-noise ratio of 30 dB, the probability of incorrect ambiguity resolution is less than 10^{-7} , therefore becoming a negligible consideration.

6.1.3 Ionospheric Error Variance

As mentioned in Section 4.4, a correction term will be introduced into the range estimate to account for the ionospheric bias. However, there will always be some difference, $\beta\Delta K$, between the actual and estimated values of ionospheric bias (Note: $\beta_B = \beta_2 b/2 \alpha_B$, $\beta_C = \beta_2 b/2 \alpha_C$). This difference, or error, contributes to the total range error. In fact, its variance adds to the error variances from the other sources because of the independence of the errors.

The magnitude of var (ionosphere) depends very intimately upon the manner in which the ionospheric bias is measured at the Ground Control Center and extrapolated to other locations. The technique to be used in this experiment is discussed in Section 4.4.2 and 4.4.3. With the present understanding of the ionosphere, a reasonable estimate for the error variance in R_1 and R_3 is 1 Km^2 . Of course, this error varies with distance between the GCC and the ionospheric links. Until more is known about the ionosphere, this error variance will be the dominant error. It is hoped that more can be learned in order to reduce this error during the experiment.

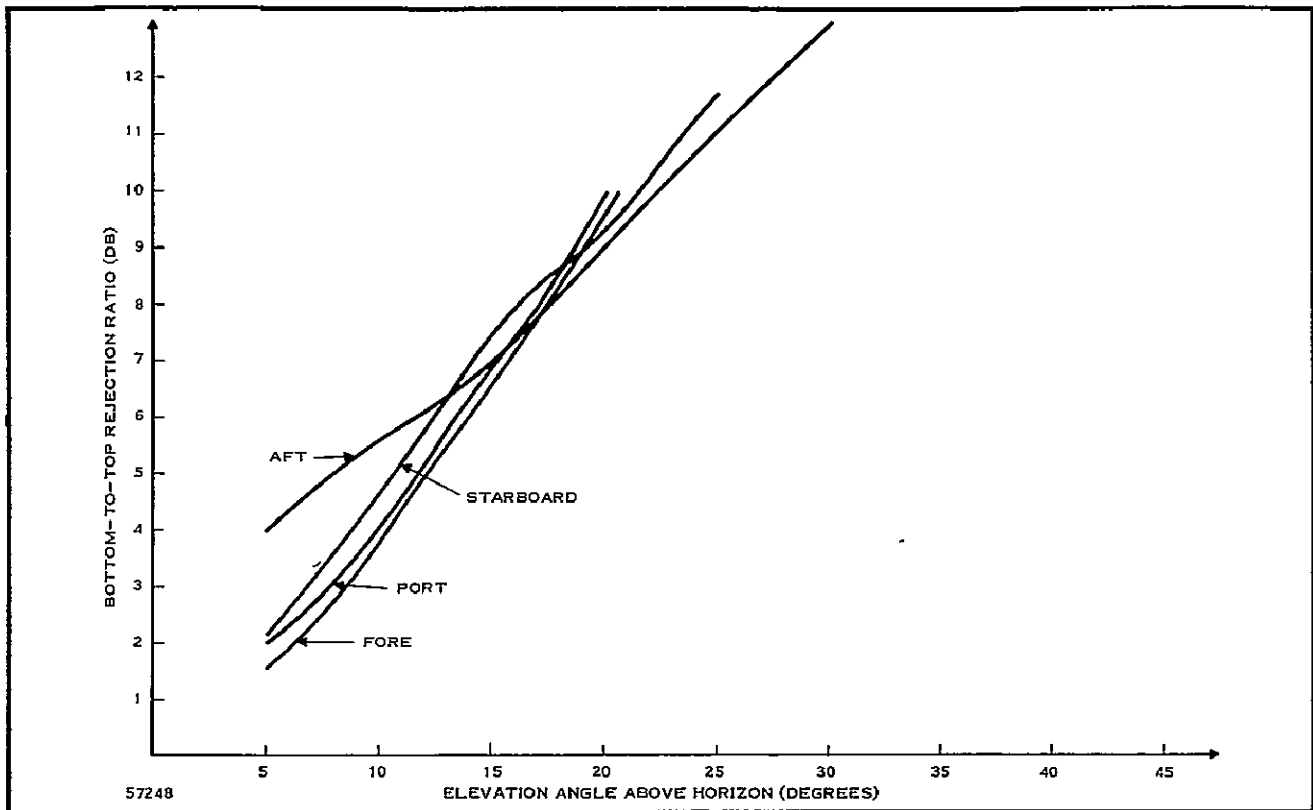


Figure 6-1. Bottom-to-Top Rejection Ratio of DMC33-2 Antenna (Horizontal Polarization)

6.1.4 Multipath Effect

The multipath effect is a potential source of range error at VHF because it is not practical to suppress the multipath signal significantly in the aircraft terminal antenna. This is especially true at low elevation angles. Clearly, a parameter directly related to the magnitude of the effect is the relative attenuation (α) of the multipath signal with respect to the direct signal. The magnitude of α is determined by the reflection coefficient of the multipath signal at the ground, and by the aircraft antenna pattern bottom-to-top rejection ratio because the satellite signal arrives above the horizon and the multipath signal arrives from below. A plot of this rejection ratio for the DMC33-2 Antenna (proposed for this experiment) when actually mounted on an aircraft is shown in Figures 6-1 and 6-2 for horizontal and vertical polarization, respectively.

At low angles of elevation, where the antenna rejection is low, the contribution to the attenuation by the multipath reflector is almost negligible over the sea, however, it may be significant for vertical polarization over land. Hence, a reasonable estimate of α for both polarizations over land is given in Figure 6-1.

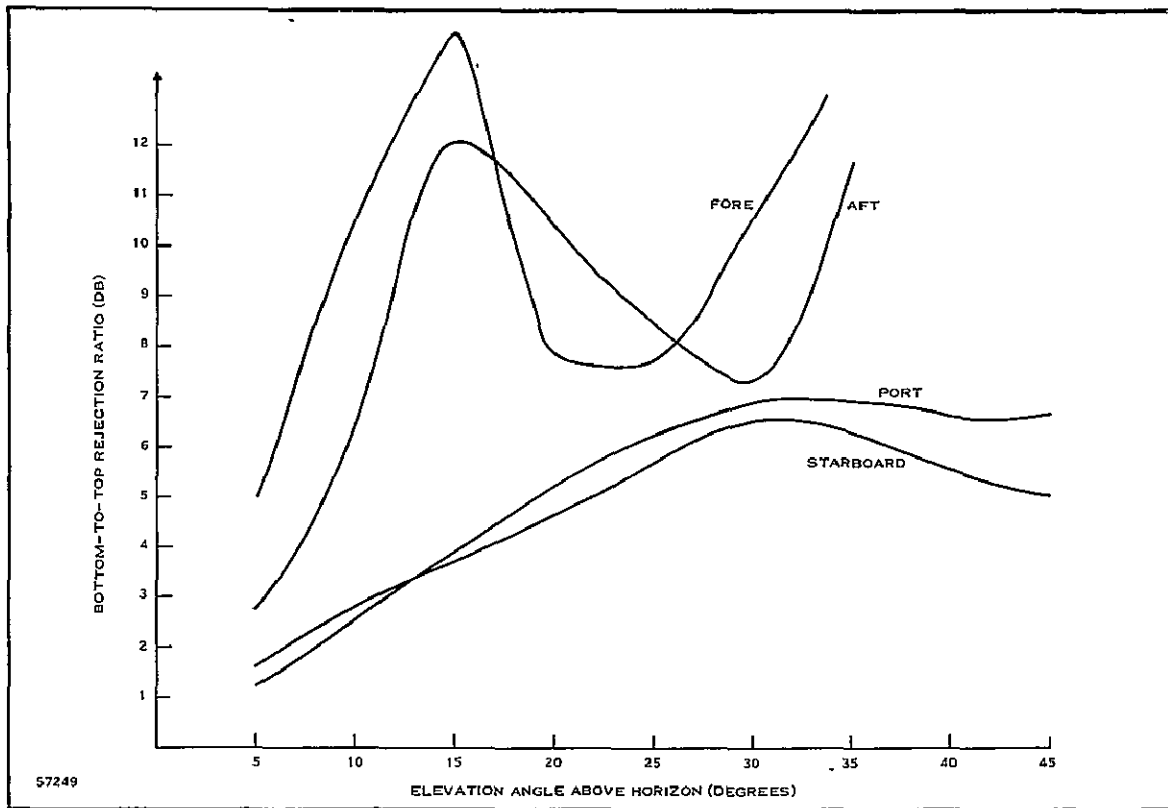


Figure 6-2. Bottom-to-Top Rejection Ratio of DMC33-2 Antenna (Vertical Polarization)

The multipath effect, as it affects ranging, need only be considered for range measurements between the satellite and the aircraft. The ground station antenna will be sufficiently low to the ground such that the differential range between the GCC and the satellite is inconsequential. However, the multipath ray may still cause cancellation at the GCC antenna, especially at low angles of elevation.

Consider the case for the satellite transmitting a carrier at ω_0 and one sidetone at $(\omega_0 + \Delta\omega_1)$. Then:

$$v_{ss} = \cos\omega_0 t + \cos(\omega_0 + \Delta\omega_1)t.$$

As received at the aircraft, the composite direct and multipath signals will be:

$$v_{ra} = \cos(\omega_0 t + \theta_{0d}) + \alpha \cos(\omega_0 t + \theta_{0m}) + \cos[(\omega_0 + \Delta\omega_1)t + \theta_{1d}] + \alpha \cos[(\omega_0 + \Delta\omega_1)t + \theta_{1m}]$$

where α is the relative attenuation of the multipath signal, the subscript d refers to the direct path, the subscript m refers to the multipath, and the phase angles are related to the ranges and frequencies by:

$$\begin{aligned}\theta_{od} &= \frac{R}{c} \omega_o & \theta_{ld} &= \frac{R}{c} (\omega_o + \Delta\omega_1) \\ \theta_{om} &= \frac{R + \Delta R}{c} \omega_o & \theta_{lm} &= \frac{R + \Delta R}{c} (\omega_o + \Delta\omega_1).\end{aligned}$$

Because each tone is finally limited and the phase difference measured, the carrier and sidetone should each be expressed as the resultant of the direct and multipath signals. Hence

$$v_{ra} = A \cos(\omega_o t + \theta_{od} + \Delta\theta_o) + B \cos\left[(\omega_o + \Delta\omega_1)t + \theta_{ld} + \Delta\theta_l\right].$$

The phase shifts shown by $\Delta\theta$ are the errors introduced in each case by the multipath signal and are given by:

$$\begin{aligned}\tan \Delta\theta_o &= \frac{\alpha \sin(\theta_{om} - \theta_{od})}{1 + \alpha \cos(\theta_{om} - \theta_{od})} = \frac{\alpha \sin \Delta\tau \omega_o}{1 + \alpha \cos \Delta\tau \omega_o} \\ \tan \Delta\theta_l &= \frac{\alpha \sin(\theta_{lm} - \theta_{ld})}{1 + \alpha \cos(\theta_{lm} - \theta_{ld})} = \frac{\alpha \sin \Delta\tau (\omega_o + \Delta\omega_1)}{1 + \alpha \cos \Delta\tau (\omega_o + \Delta\omega_1)}\end{aligned}$$

where $\Delta\tau$ is the multipath additional time delay and is $\Delta R/c$, where ΔR is the multipath range difference.

In retransmission by the aircraft terminal to the satellite, the same multipath model can be assumed to exist because the time delay is very small. Hence, the attenuation constant (α) will be unaltered. Thus, the phase difference between the sidetone and carrier on the two-way path will be just twice the one-way value, and

$$\begin{aligned}\theta_{10} &= 2\theta_{ld} + 2\Delta\theta_l - 2\theta_{od} - 2\Delta\theta_o \\ &= \frac{2R\Delta\omega_1}{c} + 2 \tan^{-1} \frac{\alpha \sin \Delta\tau (\omega_o + \Delta\omega_1)}{1 + \alpha \cos \Delta\tau (\omega_o + \Delta\omega_1)} - 2 \tan^{-1} \frac{\alpha \sin \Delta\tau \omega_o}{1 + \alpha \cos \Delta\tau \omega_o}.\end{aligned}$$

The difference in the two arctan terms is the error due to the multipath effect. It will be noted that even for α as large as 1, each arctan term will only have a maximum value of 90° , and they are nearly equal. Hence, the difference will be small. Another significant fact is that θ_{10} is integrated at the GCC over a period of 1 second, and because $\Delta\tau$ varies in that time, the error will be further attenuated.

To estimate the possible error, therefore, a distribution was assumed for $\Delta\tau$; it was assumed to be Gaussian distributed about a mean of 10 microseconds. The variance in $\Delta\tau$ was taken as 2×10^{-8} seconds and 2×10^{-7} seconds, corresponding to a differential path length change of 6 meters and 60 meters, respectively. The mean and variance of the error term were calculated for $f_0 = 150$ MHz and $\Delta f_1 = 1$ kHz. In each case, the mean was very nearly zero and the variance was a function of α . The results are plotted in Figure 6-3. It is seen that at $\alpha = 0.5$ the variance of the error is only 1.5° for a mean delay of 10 microseconds, and this corresponds to a range error of approximately 1 Km without smoothing.

The variance assumed for the differential path length change (and hence $\Delta\tau$) was estimated by observing that the multipath length will change in the period of the measurement of θ_{10} (1 second) due to the motion of the reflector point across an uneven Earth profile. This is especially so at low angles of elevation where α is high. A mean differential path length change of 6 meters was considered representative of smooth Earth conditions. Because of the relatively rapid fluctuations in the reflector profile at aircraft velocities, the small phase error will fluctuate rapidly and hence will be further attenuated by the integration used in the estimation of θ_{10} . Hence, it is concluded that for elevation angles to the satellite in excess of 5° , the multipath error will be negligible. At lower angles, the error may become significant, the final effect being determined by the spectrum of the error term as well as the factors considered here.

6.2 Altitude Measurement Error

The measurement of R_h , the distance from the Earth's center to the aircraft terminal, is the sum of the Earth's radius and the aircraft altitude. Each of these terms include errors as discussed in the Appendixes. The variance in the aircraft altitude measurement is approximately 160 m^2 , and the variance in the estimate of the Earth's radius is about 100 m^2 . The total variance in R_h is thus 260 m^2 , which is a negligible error in comparison with the errors in R_1 and R_3 , thus it will be neglected in the final position location error analysis.

6.3 Satellite Position Error

Although the positions of the satellites are assumed to be known in this position location experiment, there is some uncertainty in the precise coordinates of the satellites. The orbital plane of the ATS-1 and ATS-3 satellites are inclined 0.3° with respect to the equatorial plane. Furthermore, there is a ± 2 -Km uncertainty in the precise position location of the satellites. The maximum of this uncertainty is perpendicular to the orbital plane.

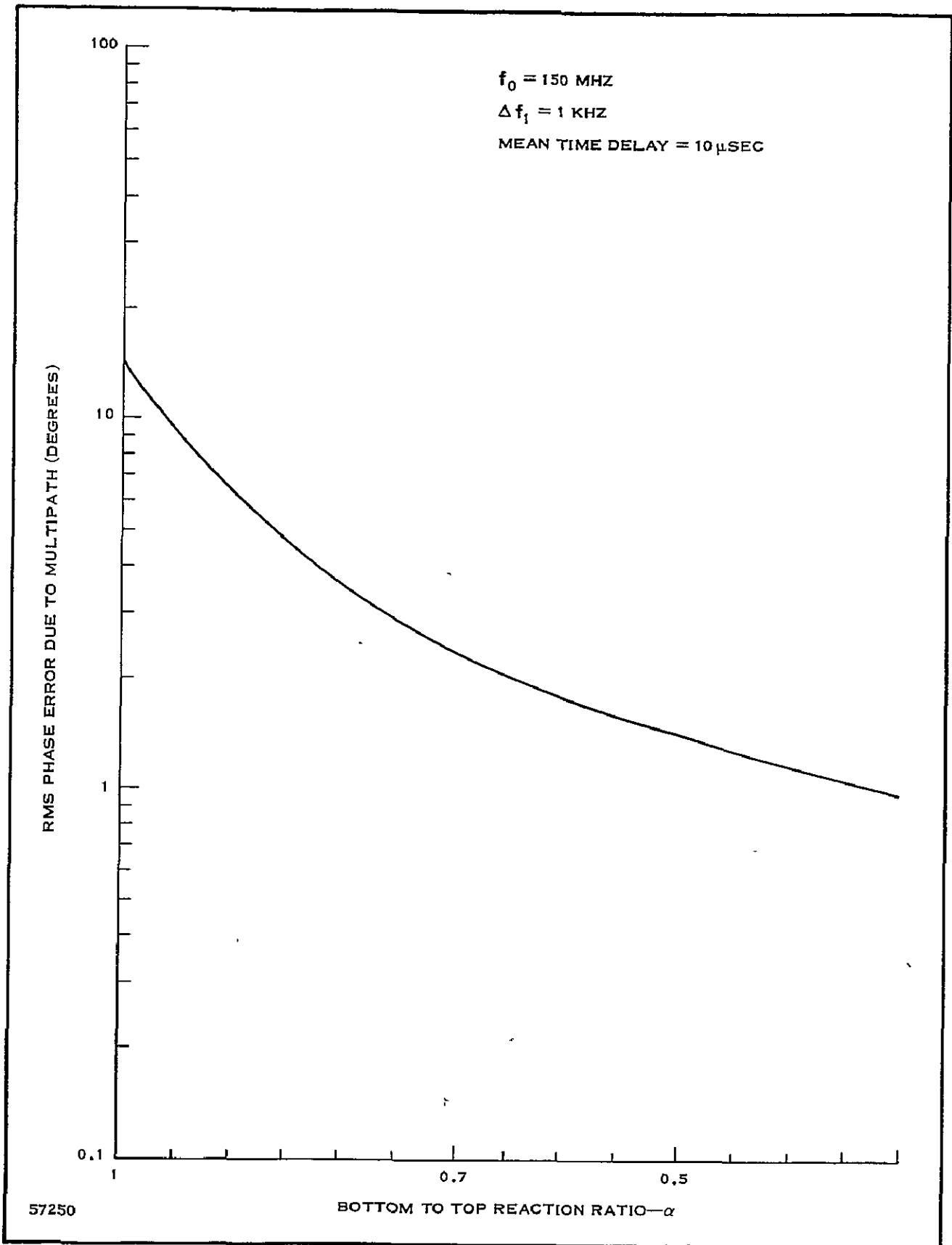


Figure 6-3. Multipath RMS Phase Error Without Smoothing

6.4 Position Location Accuracy

All of the previous discussion in Section 6.0 has been centered on the errors in range to the aircraft, the aircraft altitude, or the satellite position. However, the final and most important question is just how these various errors transform to an error in the position of the aircraft. In this section, we consider the effect of the range errors and the uncertainty of the satellite position upon the final position location accuracy.

6.4.1 Position Location Errors Due to Range Errors

In Section 5.0, the equations of the position location system were derived. Of great interest at this point is the extent to which errors in R_1 and R_3 affect the final aircraft position location accuracy. In Section 5.0, the aircraft position was defined by a position vector $\underline{R}_h = R_h \underline{b}_a$. R_h is distance from the Earth's center to the aircraft and \underline{b}_a is the three-component vector of direction cosines defining the aircraft position with respect to the Earth's center. As mentioned in Section 6.2, the error in R_h is negligible and hence is not considered here. However, the errors in R_1 and R_3 do deserve further consideration.

From Section 5.0, the changes in the first two direction cosines due to range errors are (from Equations 5.19 and 5.20):

$$\partial b_{a1} = \frac{b_{32} \partial D_1 - b_{12} \partial D_3}{\Delta} \quad (6.4.1-1)$$

$$\partial b_{a2} = \frac{b_{11} \partial D_3 - b_{31} \partial D_1}{\Delta} \quad (6.4.1-2)$$

where
$$\partial D_1 = \frac{-R_1}{R_{01} R_h} \partial R_1 \text{ and } \partial D_3 = \frac{-R_3}{R_{03} R_h} \partial R_3. \quad (6.4.1-3)$$

It also follows from the algebra of small numbers that the change in b_{a3} due to range errors is:

$$\partial b_{a3} = -\frac{1}{b_{a3}} \left[b_{a1} \partial b_{a1} + b_{a2} \partial b_{a2} + \frac{1}{2} (\partial b_{a1}^2 + \partial b_{a2}^2) \right] \quad (6.4.1-4)$$

Of great interest is the extent to which these changes in direction cosine change the latitude and longitude of the aircraft. Again, from the algebra of small numbers, the result is:

$$\partial(\text{Latitude}) = \partial b_{a3} \quad (6.4.1-5)$$

$$\partial(\text{Longitude}) = \frac{b_{a1} \partial b_{a2} - b_{a2} \partial b_{a1}}{b_{a1}^2 + b_{a2}^2} \cdot \quad (6.4.1-6)$$

It is seen from Equations 6.4.1-5 and 6.4.1-6 that the change in latitude and longitude due to range errors is a function of location. To understand the relationship between range errors and latitude-longitude changes, Equations 6.4.1-5 and 6.4.1-6 should be plotted for the locus of points covered by the two satellites. In lieu of this lengthy calculation, a value for a typical position has been calculated. A latitude of 40° N and longitude of 90° W (Central United States) and a range error of 1 Km in R₁ and R₃ yield the following results:

$$\partial b_{a1} = 1.705 \times 10^{-4}$$

$$\partial b_{a2} = -8.25 \times 10^{-5}$$

$$\partial b_{a3} = -1.435 \times 10^{-4}$$

$$\partial(\text{Latitude}) = -1.435 \times 10^{-4} \text{ radians}$$

$$\partial(\text{Longitude}) = 1.28 \times 10^{-4} \text{ radians}$$

$$\partial(\text{Latitude}) \times R = -0.915 \text{ Km}$$

$$\partial(\text{Longitude}) \times R = 0.817 \text{ Km.}$$

This result states that a 1-Km error in range transforms to a 0.915-Km change in latitude and a 0.817-Km change in longitude.

6.4.2 Position Location Errors Due to Satellite Position Uncertainty

The extent to which the ±2-Km uncertainty in the satellite position affects the aircraft position location can be seen by examining the change in the direction cosines of the aircraft position vector. This error is most easily introduced into the problem as an uncertainty in the direction cosines (b₁₃ and b₃₃) for the ATS-1 and ATS-3 satellites. From Section 5.0, the change in the direction cosines due to a change in the satellite position is given by:

$$\partial b_{a1} = -\left(\frac{b_{a3}}{b_{11}}\right) \partial b_{13} \quad (6.4.2-1)$$

$$\partial b_{a2} = -\left(\frac{b_{a3}}{b_{32}}\right) \partial b_{33} \quad (6.4.2-2)$$

$$\partial b_{a3} = \frac{b_{a1}}{b_{11}} \partial b_{13} + \frac{b_{a2}}{b_{32}} \partial b_{33} - \frac{1}{2} b_{a3} \left[\left(\frac{\partial b_{13}}{b_{11}} \right)^2 + \left(\frac{\partial b_{33}}{b_{32}} \right)^2 \right].$$

(6.4.2-3)

The ± 2 -Km maximum uncertainty in satellite position implies that $\partial b_{13} = \partial b_{33} = \pm 4.75 \times 10^{-5}$ radians. As in Section 6.4.1, it is seen that the position location error is a function of position. For the same Central United States location (40°N , 90°W) as was used in Section 6.4.1, the results are:

$$\begin{aligned} \partial b_{a1} &= \mp 7.23 \times 10^{-5} \\ \partial b_{a2} &= \mp 1.06 \times 10^{-4} \\ \partial b_{a3} &= \pm 1.51 \times 10^{-4} \\ \partial(\text{Latitude}) &= 1.51 \times 10^{-4} \text{ radians} \\ \partial(\text{Latitude}) \times R &= 0.962 \text{ Km} \\ \partial(\text{Longitude}) &= 4.24 \times 10^{-5} \text{ radians} \\ \partial(\text{Longitude}) \times R &= 0.271 \text{ Km.} \end{aligned}$$

Again, it must be remembered that these are worst-case errors for the ± 2 -Km error. Checking three points across the United States at 40°N latitude yields the following latitude/longitude worst-case errors due to satellite position uncertainty:

	40°N 75°W (East Coast)	40°N 90°W (Central U.S.)	40°N 120°W (West Coast)
$\partial(\text{Latitude}) \times R$	0.962 Km	0.718 Km	0.0942 Km
$\partial(\text{Longitude}) \times R$	0.2705 Km	0.462 Km	0.737 Km

It will be possible to remove some portion of these worst-case errors when more is known about the motion of the satellite perpendicular to the orbital planes.

7.0 MANAGEMENT

The Goddard Space Flight Center (GSFC) of the National Aeronautics and Space Administration will conduct the scientific investigation in the VHF Satellite Navigation Experiment and will produce the necessary equipment to demonstrate operational feasibility.

Responsibility for the investigation is assigned to the Data Collection Systems Section of the Communications Research Branch of the Systems Division, Goddard Space Flight Center. Mr. A.E. Jones is Chief of the Division, Mr. R.H. Pickard is Head of the Branch, and Mr. W.I. Gould is Head of the Data Collection Systems Section.

Contractors will be utilized to develop and fabricate the various equipment necessary for the experiment. Administration support is being provided through Dr. Michael J. Vaccaro, Assistant Director, Office of Administration.

The Principal Investigator is Mr. Gay E. Hilton, Senior Engineer in the Data Collection Systems Section. He is responsible for defining the overall goals of the experiment and for assuring that the various equipments are technically capable of meeting these goals.

The co-investigator is Mr. Roger Hollenbaugh, Systems Engineer in the Data Collection Systems Section. He is responsible for the system study contracts and will be the Technical Officer on one or more hardware contracts. He will also be responsible for the Data Acquisition and Data Reduction efforts.

Mr. Walter K. Allen of the Data Collection Systems Section is the Project Manager. He is responsible for the overall implementation of the VHF Satellite Navigation Experiment, including contract management and coordination of the efforts of the various groups participating in the experiment.

The Tracking and Data Systems (T and DS) Directorate is responsible for the operation of the Ground Control Center at GSFC. The T and DS Directorate will also support the data analysis requirements of the experiment. T and DS support for this experiment will be defined at a later date.

8.0 SCHEDULE

Figure 8-1 shows the schedule for the VHF Satellite Navigation Experiment. Three months' down time (9, 10, 11) is required of the OCC to incorporate the necessary modifications and to perform the system tests. These three months should correspond to a lull in the present OPLE Experiment, starting after August 1968 and ending before February 1969. After modification, the OCC will have the capability of collecting data for both experiments, however not simultaneously. A short down time in the order of a few minutes will be required to switch from one experiment to the other.

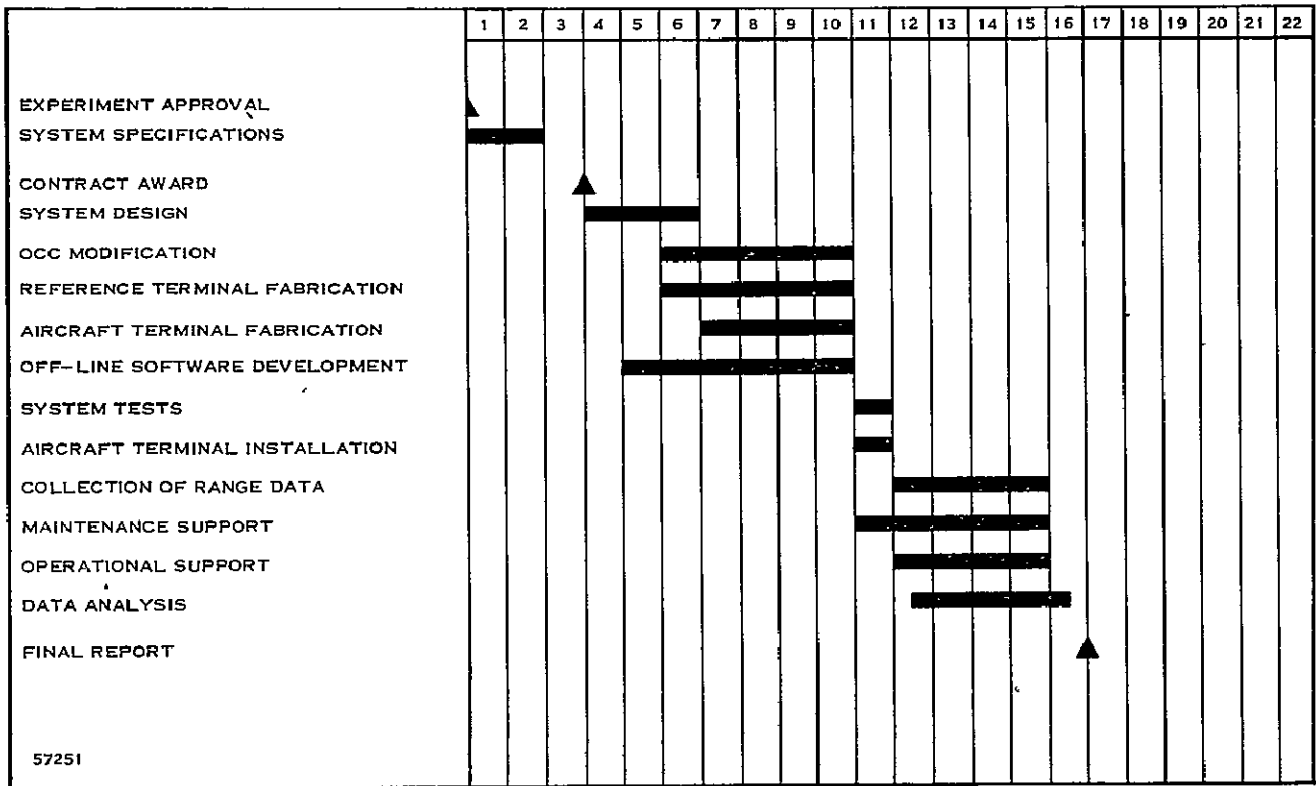


Figure 8-1. Experiment Schedule

1. Baghdady, E. J., and K. W. Kruse, "The Design of Signals for Space Communication and Tracking, " 1964 IEEE International Convention Record, Pt. 7, pp. 152-174, March 1964.
2. Laughlin, Charles, et al, "Position Location and Aircraft Communication Experiment, " NASA/Goddard Space Flight Center, May 1967.
3. Thomas, J. O., "The Electron Density Distribution in the F₂ Layer of the Ionosphere in Winter, " Journal of Geophysical Research, vol. 68, No. 9, pp. 2707 - 2718, May 1963.
4. Garriott, O. K., et al, "Observations of Ionospheric Electron Content Using a Geostationary Satellite, " Planetary Space Science, vol. 13, pp. 829-838, 1965.
5. "ATS Radio Beacon Experiment, " NASA/Goddard Space Flight Center, ATS Technical Data Report, 4.4.6.0.1 - 4.4.6.0.24.
6. Dr. da Rosa, Aldo, Private communications concerning ionospheric studies.
7. "OPLE System Power Budgets, " Technical Note OPLE-11, Contract NAS 5-10248, Communications Systems, Incorporated.

PRECEDING PAGE BLANK NOT FILMED.

APPENDIX A
A COMPARISON BETWEEN RANGING TONES
AND PN (PSEUDO-NOISE)
CODES FOR COMMERCIAL AIR
TRAFFIC CONTROL

APPENDIX A

A COMPARISON BETWEEN RANGING TONES
AND PN (PSEUDO-NOISE)
CODES FOR COMMERCIAL AIR
TRAFFIC CONTROL

A rather complete comparison between ranging tones and ranging codes for range measurements has been made by Baghdady and Kruse (Reference 1). Their conclusions are.

"First, in situations, in which there is a decisive requirement for high resolution (or precision) and minimum acquisition time, with a limitation on allowable bandwidth occupancy, systems based purely on harmonic signals (or sidetones) are potentially superior to systems based exclusively on pseudo-random codes.

"Second, in situations in which there is a decisive requirement for resolving ambiguities in excess of a lunar distance, systems based purely on pseudo-random codes are potentially superior to those based on continuous tones.

"Third, from the viewpoint of all considerations influenced decisively by bandwidth occupancy, systems based exclusively on continuous tones are potentially preferable to those based exclusively on pseudo-random codes.

"Fourth, in situations in which there is a decisive requirement for transmission security and jam resistance, pseudo-random codes are clearly more advantageous.

"Fifth, in all other respects than those just enumerated, the two types of systems are of comparable ratings."

Reviewing these points with respect to this VHF Satellite Navigation Experiment, we find that the first point favors the harmonic signals from the standpoint of high resolution, minimum acquisition time, and minimum bandwidth occupancy. The acquisition scheme with the tones is just an algorithm which can be performed very quickly by a digital computer as opposed to acquisition by the decoding hardware for the pseudo-random codes. If many individual aircraft ranges are to be determined, as in an operational system, this savings in acquisition time provided by the harmonic signals can become quite significant.

Because the distances involved in aircraft navigation via synchronous satellite are much less than lunar distances, the ambiguity resolution of harmonic signals is quite adequate.

As far as bandwidth and resolution is concerned, Baghdady points out that the autocorrelation function of the highest frequency sinusoid (f_h Hz) has a width of $1/2 f_h$ at the base of each lobe. For rectangular pulses of width Δt seconds, the width of the base of the autocorrelation function at the zero crossing point is $2 \Delta t$. Now, consider rectangular pulses of width Δt for which the minimum bandwidth is $8/\Delta t$ in order that rectangular pulses are preserved. Also, consider a sinusoid of frequency $f_h = 8/\Delta t$ Hz, the base of its autocorrelation function is $1/2 f_h = \Delta t/16$. Because the rectangular pulses have an autocorrelation function whose width is $2\Delta t$, the sinusoid has a factor of $2\Delta t/(\Delta t/16) = 32$ improvement in resolution over that of the pseudo-random code which fully occupies the $8/\Delta t$ bandwidth. The sinusoid occupies a discrete frequency thereby permitting the adjacent frequency spectrum to be utilized for other purposes.

In commercial air traffic control, secure communications are unnecessary, hence harmonic signals can be used. Thus, concerning the five points made by Baghdady with respect to commercial aircraft navigation, ranging by harmonic tones is potentially preferable to ranging by pseudo-random codes.

REFERENCES

1. Baghdady, E.J., and K. W. Kruse, "The Design of Signals for Space Communications and Tracking," 1964 IEEE International Convention Record, Part 7, pp. 152-174, March, 1964.

APPENDIX B
ATMOSPHERIC BIAS ERRORS IN VHF RANGING

APPENDIX B

ATMOSPHERIC BIAS ERRORS IN VHF RANGING

1.0 INTRODUCTION

The sidetone ranging technique described herein measures the phase delay between transmitted and received tones (sinusoids). The phase delay is directly proportional to the range between the transmitter and receiver, thus it yields a range estimate. However, the troposphere and ionosphere alter the phase delay from its free space value thereby introducing bias errors into the range estimate. It is the purpose of this appendix to show the relations between the estimated range, the phase delay or shift, and the bias errors. Where possible the equations are written to describe the sidetone ranging just as it will be done by the Ground Control Center in cooperation with the ATS satellites.

A thorough study of electromagnetic wave propagation through the atmosphere under all parametric conditions is a very complex task. To simplify this task, atmospheric models (References 1, 2, and 3) which adequately represent average conditions are employed to estimate the effect of the Earth's atmosphere upon range measurements. These models indicate that the phase delay of a sidetone is directly related to the index of refraction of the propagation medium.

2.0 PHASE DELAY DUE TO THE ATMOSPHERE (TROPOSPHERE AND IONOSPHERE)

The phase path length of a VHF radio path between a ground station and satellite is given by (Reference 4):

$$P(\text{meters}) = \int_1^2 \mu dl \quad (\text{B-1})$$

where μ is the index of refraction of the medium along the ray path. This index differs from unity primarily in the troposphere (0 to 30.5 Km) and the ionosphere (85 to 1000 Km). Hence, Equation (B-1) can be rewritten as:

$$P = \int_1^{12} (1 + \Delta \mu_{\text{trop}}) dl + \int_{12}^{13} (1) dl + \int_{13}^{14} (1 - \Delta \mu_{\text{ion}}) dl + \int_{14}^2 (1) dl$$

$$P = \int_1^2 (1) dl + \int_1^{12} \Delta \mu_{\text{trop}} dl - \int_{13}^{14} \Delta \mu_{\text{ion}} dl \quad (\text{B-2})$$

where (1, 12) and (13, 14) denote the lower and upper limits of the troposphere and ionosphere, respectively. The first integral on the right hand side of Equation (B-2) is just the path length, R_{gs} , while the other integrals can be extended to the limits 1 to 2 because $\Delta \mu_{trop}$ and $\Delta \mu_{ion}$ differ from zero only in the troposphere and ionosphere, respectively. The subscript gs on R_{gs} indicates that the range of interest is the ground station/satellite range. Equation (B-2) can now be written as:

$$P = R_{gs} + \int_1^2 \Delta \mu_{trop} dl_1 - \int_1^2 \Delta \mu_{ion} dl_2 \quad (B-3)$$

$$P = R_{gs} + \csc \psi \int_{h_1}^{h_2} \Delta \mu_{trop} dh - \csc \alpha_1 \int_{h_1}^{h_2} \Delta \mu_{ion} dh \quad (B-4)$$

where $dl_1 = \csc \psi dh$, and $dl_2 = \csc \alpha_1 dh$

and $h_1 =$ height of ground or aircraft transmitter above sea level

$h_2 =$ height of satellite above sea level.

The angle ψ is the ray's elevation angle at ground level whereas α_1 is the ray's elevation angle at the middle of the ionosphere. Because of the Earth's curvature, they are not the same, but they can be related by (Reference 5):

$$\alpha = \cos \alpha_1 = (1 - 0.928 \cos^2 \psi)^{-1/2}. \quad (B-5)$$

The phase delay in cycles is given by:

$$\theta(\text{cycles}) = \frac{P}{\lambda} = \frac{f}{c} P. \quad (B-6)$$

Substituting (B-4) into (B-6) yields:

$$\theta(\text{cycles}) = \frac{f}{c} \left[R_{gs} + (\csc \psi) \Delta s_{trop} - (\csc \alpha_1) \Delta s_{ion} \right] \quad (B-7)$$

where

$$\Delta s_{trop} = \int_{h_1}^{h_2} \Delta \mu_{trop} dh$$

and

$$\Delta s_{ion} = \int_{h_1}^{h_2} \Delta \mu_{ion} dh. \quad (B-8)$$

The Appleton-Hartree equation gives $\Delta\mu_{ion}$ as a power series in ω^{-1} . Consideration of the first-order term is usually adequate, and hence Δs_{ion} becomes:

$$\Delta s_{ion}(m) = \frac{b}{\omega^2} \int_{h_1}^{h_2} Ndh \quad (B-9)$$

where $b = 1.6 \times 10^3$ mks units

ω = radian frequency of signal

N = electron density of ionosphere (electrons/m³).

$\Delta\mu_{trop}$ is independent of frequency but does depend upon the tropospheric temperature, the total pressure, and the partial pressure of the water vapor.

3.0 RANGE ESTIMATION USING THE PHASE DELAY OF THE SIDETONES

The ranges of interest in this position location system are R_1 and R_3 , the aircraft-to-satellite ranges, as shown in Figure B-1. R_1 and R_3 cannot be measured directly, but instead are derived from a combination of measurements given by:

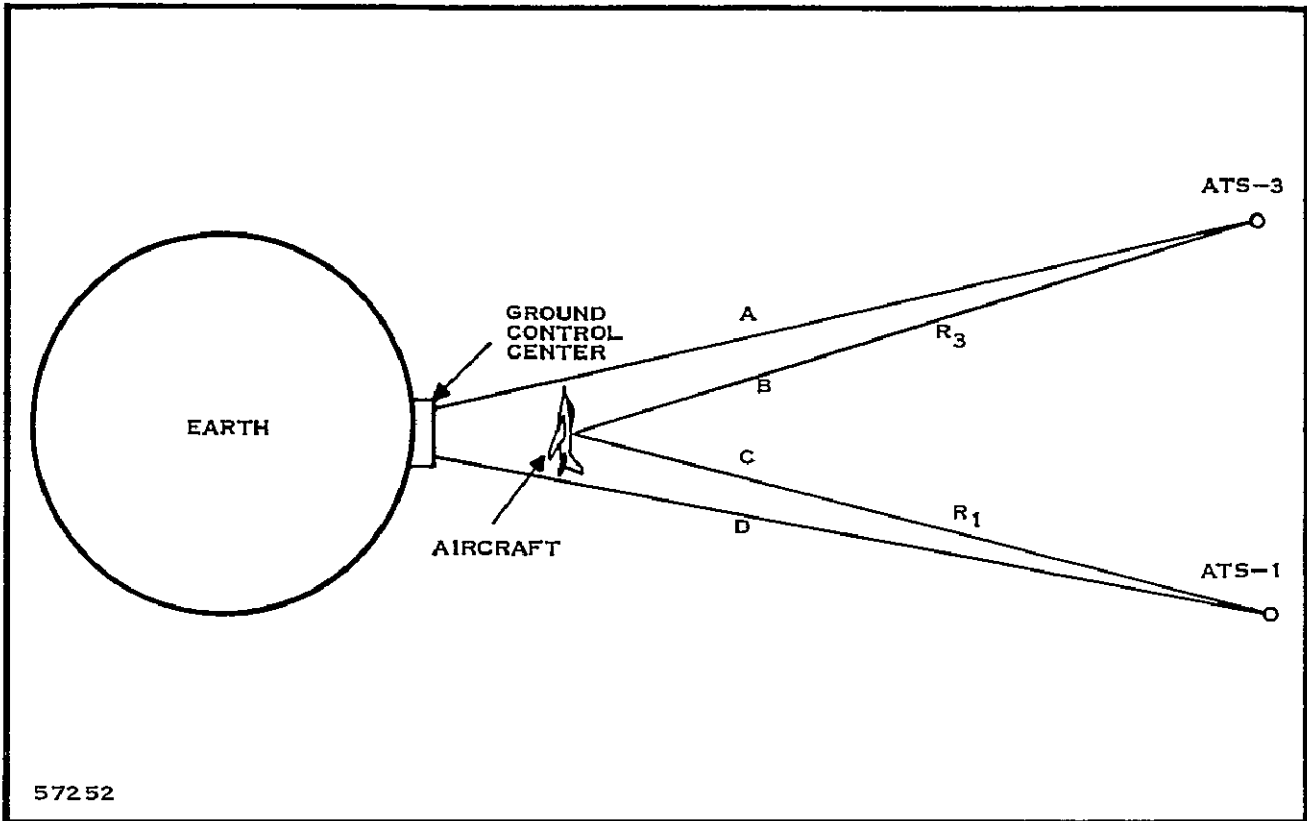
$$R_3 = 1/2 (R_{g3a3g} - R_{g3g}) \quad (B-10)$$

$$R_1 = R_{g3a1g} - 1/2 (R_{g3a3g} + R_{g1g}) \quad (B-11)$$

where the subscripts denote the range of interest. For example, R_{g3a3g} is the GCC/ATS-3/aircraft/ATS-3/GCC path distance. All of these terms refer to a path traversed by the sidetone in making a round trip from the GCC to a satellite or aircraft.

Range R_{g3g} is estimated by measuring the phase delay of a signal that is sent to the ATS-3 satellite and returned to the Ground Control Center. The round trip phase delay experienced by the reference tone (A/R tone) is.

$$\theta_{1g3g} = \frac{f_{1U}}{c} \left[R_{g3} + \csc\psi_A \Delta s_{tropA} - \alpha_A \frac{b}{\omega_{1U}^2} \int_{h_1}^{h_2} Ndh \right] + \frac{f_{1D}}{c} \left[R_{3g} + \csc\psi_A \Delta s_{tropA} - \alpha_A \frac{b}{\omega_{1D}^2} \int_{h_1}^{h_2} Ndh \right] \quad (B-12)$$



57252

Figure B-1. Relationship Between Ground Control Center, Satellites, and Aircraft

where

$$\omega_{1U} \approx 149.22 \times 2\pi \times 10^6 \text{ rad/sec}$$

$$\omega_{1D} \approx 136.6 \times 2\pi \times 10^6 \text{ rad/sec.}$$

NOTE: Subscript A refers to path A in Figure B-1.

The slight frequency offset of the A/R tone from the carrier frequency is negligible when calculating ω^{-1} or ω^{-2} . Later, when $f_{2U} - f_{1U}$ is used, an exact difference can be obtained.

The phase delay of another signal is measured in a similar manner. For example, consider the simulated 10.2-kHz Omega signal which is placed 426.428057 Hz above the A/R tone in the frequency spectrum. Its phase delay is:

$$\theta_{2g3g} = \frac{f_{2U}}{c} \left[R_{g3} + \csc \psi_A \Delta s_{tropA} - \alpha_A \frac{b}{\omega_{2U}^2} \int_{h_1}^{h_2} N dh \right] + \frac{f_{2D}}{c} \left[R_{3g} + \csc \psi_A \Delta s_{tropA} - \alpha_A \frac{b}{\omega_{2D}^2} \int_{h_1}^{h_2} N dh \right]. \quad (B-13)$$

For ease of notation, let

$$K_A = \int_{h_1}^{h_2} Ndh \text{ along path A.} \quad (\text{B-14})$$

The difference between the phase delays for two distinct frequencies is the phase delay for a ranging sidetone at the difference frequency. The result is

$$\theta_{21g3g} = \frac{\Delta f_{21}}{c} \left[R_{g3g} + 2 \csc \psi_A \Delta s_{tropA} + \alpha_A^b \beta_2 K_A \right] \quad (\text{B-15})$$

where

$$\beta_2 = \left[\frac{1}{\omega_{1U} \omega_{2U}} + \frac{1}{\omega_{1D} \omega_{2D}} \right] \quad (\text{B-16})$$

and

$$\Delta f_{21} = f_{2U} - f_{1U} = f_{2D} - f_{1D} = 426.428057 \text{ Hz.}$$

The phase delays for the other two ranging sidetones are

$$\theta_{31g3g} = \frac{\Delta f_{31}}{c} \left[R_{g3g} + 2 \csc \psi_A \Delta s_{tropA} + \alpha_A^b \beta_3 K_A \right] \quad (\text{B-17})$$

$$\theta_{41g3g} = \frac{\Delta f_{41}}{c} \left[R_{g3g} + 2 \csc \psi_A \Delta s_{tropA} + \alpha_A^b \beta_4 K_A \right] \quad (\text{B-18})$$

where

$$\Delta f_{31} = 706.905276 \text{ Hz}$$

$$\Delta f_{41} = 941.428057 \text{ Hz}$$

$$\beta_3 = \left(\frac{1}{\omega_{3U} \omega_{1U}} + \frac{1}{\omega_{3D} \omega_{1D}} \right) \quad (\text{B-19})$$

$$\beta_4 = \left(\frac{1}{\omega_{4U} \omega_{1U}} + \frac{1}{\omega_{4D} \omega_{1D}} \right)$$

$$\omega_{4U} \approx \omega_{3U} \approx \omega_{1U} \approx 149.22 \times 2\pi \times 10^6 \text{ rad/sec}$$

$$\omega_{4D} \approx \omega_{3D} \approx \omega_{1D} \approx 135.6 \times 2\pi \times 10^6 \text{ rad/sec.}$$

The relation between the A/R tone and the sidetones in one of the 2.5-kHz channels is shown in Figure B-2.

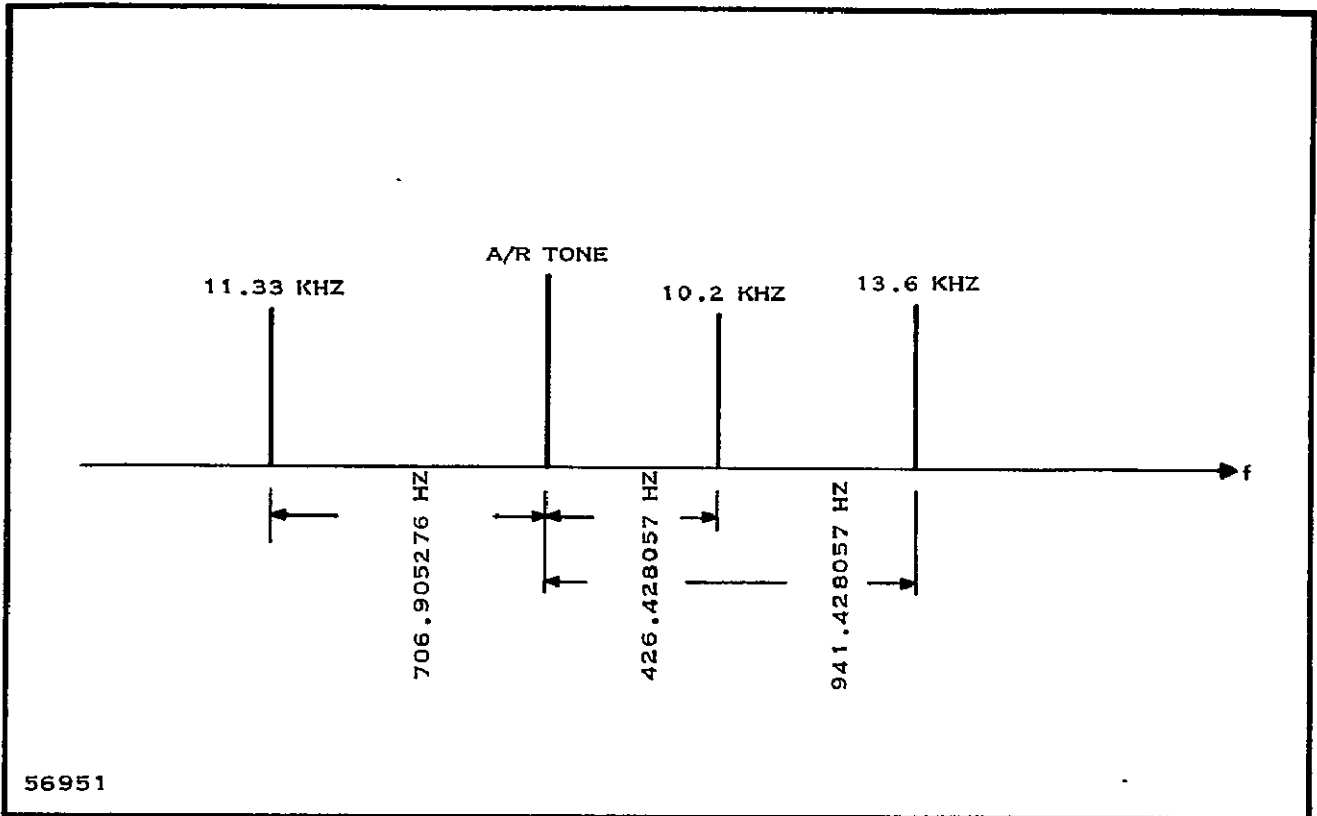


Figure B-2. Frequency Spectrum of One 2.5-kHz Channel

Because the phase measurement of θ_{21g3g} is an angle between zero and one cycle, the other two phases, θ_{31g3g} and θ_{41g3g} , are combined in an ambiguity resolution scheme to determine the proper number of whole cycles associated with each range measurement.

The phase delay of the Δf_{21} ranging sidetone along the path R_{g3a3g} is:

$$\theta_{21g3a3g} = \frac{\Delta f_{21}}{c} \left[R_{g3a3g} + 2csc\psi_A \Delta s_{tropA} + 2csc\psi_B \Delta s_{tropB} + \beta_2 b \left(\alpha_A K_A + \alpha_B K_B \right) \right]. \quad (B-20)$$

Using (B-10), (B-13), and (B-20) to determine R_3 yields:

$$R_3 = 1/2 \left(R_{g3a3g} - R_{g3g} \right)$$

$$\hat{R}_3 = \frac{c}{2 f_{21}} \left(\theta_{21g3a3g} - \theta_{21g3g} \right) - csc\psi_B \Delta s_{tropB} - \beta_2 \frac{b}{2} \alpha_B K_B. \quad (B-21)$$

Range estimates of R_3 can also be made using the phase shifts at sidetones Δf_{31} and Δf_{41} . The result is the same as that shown in Equation (B-21) for sidetone Δf_{21} except that the subscripts 21 become 31 or 41 and β_2 becomes β_3 or β_4 , respectively.

Repeating the above procedure, range estimates for R_1 can be derived based on Equation (B-11). The range estimate R_1 made by Δf_{21} sidetone is

$$\hat{R}_1 = \frac{\Delta f_{21}}{c} \left(\theta_{21g3a1g} - 1/2 \theta_{21g3a3g} - 1/2 \theta_{21g1g} \right) - \text{csc } c \Delta s_{\text{trop } c} - \beta_2 \frac{b}{2} \alpha_c K_c . \quad (\text{B-22})$$

The range estimates of R_1 based upon the other sidetones (Δf_{31} and Δf_{41}) follow immediately.

There are methods of combining the three range estimates in such a way that the errors in the new estimate is less than the error in any individual range estimate. Furthermore, possibilities exist for removing the atmospheric bias. These are discussed elsewhere in the text.

REFERENCES

1. Anway, A. C., "Empirical Determination of Total Atmospheric Refraction at Centimeter Wave Lengths by Radiometric Means," NBS J. Res., ser. D, 67 D (2), pp. 153-160, March-April 1963.
2. Bean, B. R., and G. D. Thayer, "Comparison of Observed Atmospheric Radio Refraction Effects with Values Predicted Through Use of Surface Weather Observations," NBS J. Res., ser. D, 67 D (3), pp. 273-285, May-June 1963.
3. Bean, B. R., and G. D. Thayer, "CRPL Exponential Reference Atmosphere," NBS, Monograph, no. 4, October 29, 1959.
4. Lawrence, R. S., C. G. Little, and H. J. Chivers, "A Survey of Ionospheric Effects Upon Earth-Space Radio Propagation," IEEE Proc., vol. 52, pp. 4-26, January 1964.
5. "Technological Considerations Concerning Satellite Communication Systems," Hughes Aircraft Company, Report R-73, October 1958.

PRECEDING PAGE BLANK NOT FILMED.

APPENDIX C
DISTANCE FROM THE AIRCRAFT TO THE
CENTER OF THE EARTH

DISTANCE FROM THE AIRCRAFT TO THE
CENTER OF THE EARTH

1.0 INTRODUCTION

In the VHF Satellite Navigation Experiment, ranging measurements to an aircraft are made from two geostationary satellites. After proper range ambiguity resolution, two spheres of position are obtained, one centered at each satellite. A third sphere of position can be obtained by determining the distance from the aircraft to the center of the Earth.

The determination of this third sphere of position is discussed here. It is assumed that the true altitude above mean sea level, h_t , has been measured accurately with a barometric altimeter or by other means and that the geodetic latitude of the aircraft is known.

2.0 DEFINITIONS (Jeffreys, THE EARTH, Cambridge University Press, London, 1959.)

Geoid: The locus of points below the Earth's surface equal to the measured height. It coincides with the mean sea level surface on the oceans.

Referenced spheroid The ellipsoid of revolution which most nearly approximates the mean sea level surface of the Earth. It is characterized by the equatorial radius R_e and the flattening f , where:

$$f^{-1} = \frac{R_e}{R_e - R_p}$$

and R_p is the polar radius.

Altitude h_t : The height above the geoid (or mean sea level surface) and is measured perpendicular to the reference spheroid.

Geodetic latitude ϕ : The angle between the equatorial plane and the normal to the reference spheroid at the station. Geodetic latitude is indicated on maps.

Geocentric latitude θ (declination): The angle between the equatorial plane and the radius vector to the station.

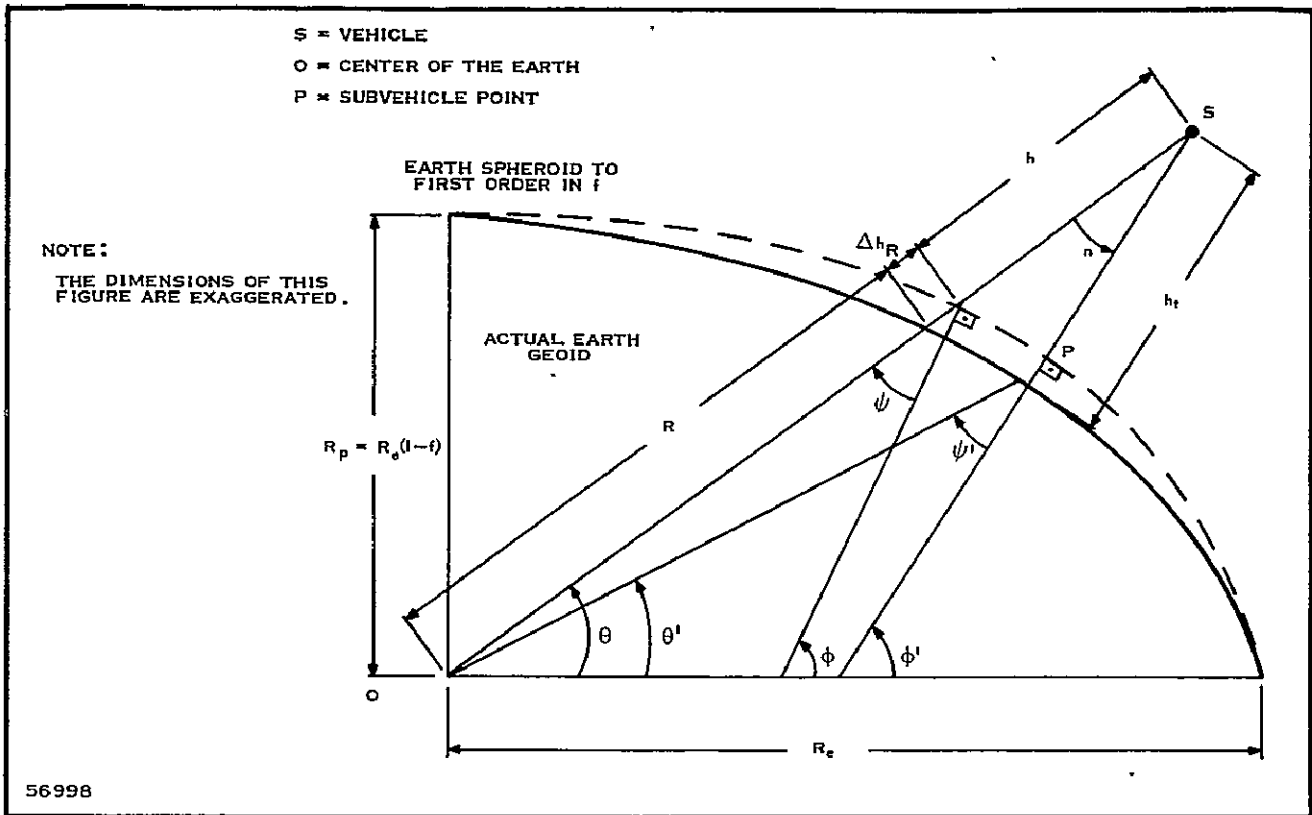


Figure C-1. Vehicle Altitude with Respect to Earth Geometry

Vehicle position (θ , ϕ): The geocentric and geodetic latitude of the vehicle S are the geocentric latitudes of the subvehicle point, or the point P, defined by erecting a perpendicular at the reference spheroid which passes through S.

3.0 DISCUSSION (Refer to Figure C-1)

The error involved in calculating the airplane's geocentric radius (r) from its altitude by use of the equation:

$$r = h + R(\theta) \quad (C-1)$$

$$\text{where } R(\theta) \approx R_e (1 - f \sin^2 \theta) \quad (C-2)$$

is due to three causes. These are:

- (1) The approximation involved in describing the reference spheroid to first order in f ;
- (2) The approximation involved in defining the altitude along the radius vector rather than the vertical to the reference spheroid;

- (3) The difference between the geoid and a reference spheroid with a specified flattening.

The reference spheroid is given by

$$\frac{R^2 \cos^2 \theta}{R_e^2} + \frac{R^2 \sin^2 \theta}{R_e^2 (1-f)^2} = 1 \quad (C-3)$$

from which

$$R = R_e (1-f) \left[1 - (2f-f^2) \cos^2 \theta \right]^{-1/2} . \quad (C-4)$$

Equation C-4 can be written for small f:

$$R \simeq R_e \left[1 - f \sin^2 \theta - 3/8 f^2 \sin^2 2\theta + 0(f^3) \right] . \quad (C-5)$$

The second-order term in Equation C-5 has a value of:

$$\Delta h_R = 3/8 f^2 R_e \sin^2 2\theta = 26.9 \sin^2 2\theta \text{ [m]} . \quad (C-6)$$

Thus, the altitude error in describing the reference spheroid to first order in f has a maximum value of 26.9m at $\theta = 45$ degrees.

The geocentric latitude (θ) of a point on the spheroid is related to its geodetic latitude (ϕ) by:

$$\begin{aligned} \tan (\phi - \theta) &= \frac{1}{R} \frac{dR}{d\theta} \\ &= \frac{R_e}{R} \left[f \sin 2\theta + \frac{3}{4} f^2 \sin 4\theta + 0(f^3) \right] \end{aligned} \quad (C-7)$$

and to first order in f.

$$\tan \psi = \tan (\phi - \theta) = f \sin 2\theta . \quad (C-8)$$

The angle ψ has a maximum value of.

$$\psi_{\max} = (\phi - \theta)_{\max} \simeq 0.192 \text{ degrees at } \theta = 45 \text{ degrees.} \quad (C-9)$$

One can see from Figure C-1 that for $\theta = 45$ degrees, $\psi > \psi' > \eta$, and the maximum altitude error due to the error in the vertical to the reference spheroid is approximately:

$$\Delta h_\eta = h(1 - \cos \eta) < h(1 - \cos \psi) \simeq h \frac{\psi^2}{2} \quad (C-10)$$

with a maximum value of 5.6×10^{-6} at $\theta = 45$ degrees. For aircraft altitudes, this amounts to fractions of a meter and can safely be neglected.

The difference in height (Δh_G) between the geoid and reference spheroid depends on the parameters of the reference spheroid. For instance, Kaula in 1961 (Reference 1) quotes differences between -51m and $+43\text{m}$, although more recent geodetic and gravimetric data should be utilized.

For the VHF Satellite Navigation Experiment, it is recommended that the maximum error in airplane radius calculation be limited to $\pm 10\text{m}$ (33 ft) so that the calculations are significantly more accurate than the observed data. The expressions for the airplane radius should hence be

$$r = h_t + R_e (1 - f \sin^2 \theta - 3/8 f^2 \sin^2 2\theta) + \Delta h_G \quad (\text{C-11})$$

where h_G can be tabulated and stored for the Earth as a function of latitude and longitude. It is important that the values of R_e , f , and Δh_G be consistent and that agreement be reached on their values.

Because in general the geodetic latitude of the aircraft is known rather than the declination, an approximate value of θ can be obtained from Equation C-8 by noting that:

$$\tan(\phi - \theta) \simeq \phi - \theta \text{ for small } (\phi - \theta)$$

and the error introduced in replacing θ by ϕ on the righthand side of Equation C-8 is of order f^2 which yields an error of order f^3 in Equation C-11. Thus, Equation C-8 can be written approximately

$$\theta = \phi - f \sin 2\phi. \quad (\text{C-12})$$

The error in airplane radius introduced by using ϕ instead of the more correct ϕ' in Equation C-12 is negligible.

4.0 SUMMARY

Given values of h_t and ϕ' , the airplane distance from the center of the Earth can be determined to within $\pm 10\text{m}$ by use of the expressions:

$$\begin{aligned} \theta &= \phi' - f \sin 2\phi' \\ r &= h_t + R_e (1 - f \sin^2 \theta - 3/8 f^2 \sin^2 2\theta) + \Delta h_G. \end{aligned}$$

It has been assumed that the difference (Δh_G) between the geoid and reference spheroid is known to about $\pm 5\text{m}$ along the flight path of the airplane. A detailed analysis of more recent data is required to determine appropriate values of R_e , f , Δh_G and the uncertainty associated with these values when the VHF Satellite Navigation Experiment will be performed.

5.0 REFERENCES

- (1) "A Geoid and World Geodetic System Based on a Combination of Gravimetric, Astrogeodetic and Satellite Data," NASA TND-702, Washington, D. C., May 1961.

PRECEDING PAGE BLANK NOT FILMED.

APPENDIX D
ALTITUDE MEASUREMENT ERRORS

PRECEDING PAGE BLANK NOT FILMED.
APPENDIX D

ALTITUDE MEASUREMENT ERRORS

The primary instrument for measuring an aircraft's altitude is the barometric altimeter. Because, measurement of altitude is part of the determination of a third sphere of position in the VHF Satellite Navigation System, an evaluation of altitude measurement errors is required for the estimation of position location accuracy. The aircraft is assumed to be a commercial, high-speed, subsonic turbojet and the following material has been obtained from Reference 1.

- (1) The system error in measuring altitude is considered to be the statistical sum of the instrument error and the static pressure error.
- (2) The instrument error is due to drift, friction, temperature, hysteresis, and similar mechanical causes as well as the interpretation of the altitude and pressure setting scales by the pilot.
- (3) The static pressure error is the difference between the free-stream static pressure and the pressure indicated by the pitot tube or fuselage vent due to compressibility and flow effects. The static pressure error can be further sub-divided into a fixed error for a given aircraft type (this fixed error can be partially compensated for) and a random error.

The precision altimeter instrument error (three-sigma value) was estimated in Reference 2 to be 132 ft, as recommended by the IATA and ICAO, the specified accuracy of air data compensators is usually given as 0.2 percent of altitude (i. e., 70 ft at 35,000 ft). Variable static pressure errors have been estimated by IATA to be 250 ft between 30,000-ft and 50,000-ft altitudes. These error estimates seem to be borne out by flight tests described in Reference 1, and it is assumed that they are three-sigma values.

System errors were obtained by making pressure altitude and radio altimeter measurements between two pairs of aircraft on routine flights over the North Atlantic at altitudes above 29,000 ft (Reference 3). Data reduction yielded a three-sigma error of 510 ft for a pair of aircraft and a calculated error value of 360 ft for a single aircraft. In Reference 2, three-sigma system errors of 342 ft were estimated for aircraft using uncorrected precision altimeters and 279 ft for aircraft using servo-corrected precision altimeters.

REFERENCES

1. Gracey, William, "Recent Developments in Pressure Altimetry," *Journal of Aircraft*, vol. 2, May-June 1965.
2. "Summary of the Work of the Vertical Separation Panel," ICAO Report VSP-WO/57, Montreal, Canada, February 15, 1961.
3. "Report on Pressure Altimeter System Accuracy Study, North Atlantic Region, July-August 1962," IATA, Montreal, Canada, 1962.